coatings

MDPI

Article

Pigments, Colouring Techniques and Tibetan Esoteric Buddhist Color Canons: A Study on Murals in Mogao Cave 465 at Dunhuang

Dandan Li, Jinli Zhao, Yaopeng Yin and Zongren Yu *

Conservation Institute, Dunhuang Academy, Dunhuang 736200, China; ldd20397@dha.ac.cn (D.L.); zhaojinli1988@163.com (J.Z.); yinyp@dha.ac.cn (Y.Y.)
* Correspondence: yuzr@dha.ac.cn

Abstract

This study investigates the Esoteric Buddhist murals in Cave 465 of the Mogao Caves, Dunhuang. Widespread discolouration renders the present colours black, grey, dark-toned or mottled white. Previous iconographic identifications relied solely on morphological features such as mudras, postures and ritual implements, without supporting colour evidence. Microscopic and spectroscopic analyses were undertaken to identify pigments, characterise colouring techniques and infer the original colours. The inferred colour data were compared with textual iconographic prescriptions and conventional Thangka colour schemes to explore their correlations. The murals utilise mineral pigments including hematite, red lead, cinnabar, orpiment, realgar, azurite, atacamite, gypsum and calcite, alongside the organic pigment lac dye. Superimposed painting, glazing and colour mixing were widely adopted. The colour schemes of the Five Dhyani Buddhas, several Vajra deities and their consorts, and protective deities show similarities to textual records, while blue pigments were applied in more diverse and complex ways, yielding not a uniform blue but blues of varied tones. The results of this study provide colour evidence for deity identification in Cave 465, an important reference for research on Tantric Buddhist imagery in the Dunhuang grottoes, and a scientific basis for mural colour reconstruction.

Keywords: Mogao cave 465; mural paintings; spectroscopic analysis; colouring techniques; color canons of Tibetan Buddhist painting

Academic Editors: Aurora Martínez-Corral and María-Elena Rodrigo-Clavero

Received: 24 September 2026
Revised: 30 October 2026
Accepted: 6 November 2026
Published: 12 November 2026

Copyright: © 2026 by the authors. Licensee MDPI, Basel, Switzerland. This article is an open access article distributed under the terms and conditions of the Creative Commons Attribution (CC BY) license.

1. Introduction

The Mogao Caves are located on the eastern cliff face of Mingsha Mountain, approximately 25 km southeast of Dunhuang City, Gansu Province, China. As a world-renowned repository of Buddhist art along the ancient Silk Road, the Mogao Caves constitute an invaluable cultural heritage site. According to historical records, the construction of the Mogao Caves began in AD 366, when the monk Lè Zūn initiated the excavation of the first cave. Subsequent construction continued for more than a millennium through successive dynasties and historical periods, including the Sixteen Kingdoms, Northern Dynasties, Sui, Tang, Five Dynasties, Song, Western Xia, and Yuan dynasties. In 1987, the Mogao Caves were inscribed on the UNESCO World Heritage List.

The Mogao Caves currently comprise 735 numbered caves, of which 492 contain surviving mural paintings and polychrome sculptures. The murals cover approximately

45,000 m², while 2415 painted sculptures are preserved at the site. Among them, Cave 465 is the only extant cave at the Mogao Caves that preserves a complete visual program of Tibetan Esoteric Buddhism belonging to the Anuttarayoga Tantra tradition. The cave was constructed in either the Western Xia or Mongol-Yuan period. It contains a rich and systematic corpus of Esoteric Buddhist murals, encompassing a wide range of tantric deities, including principal deities, Buddhas, the Vajras and their consorts, and Dharmapālas [1]. These murals constitute key material evidence for investigating the iconographic system, ritual traditions, and artistic practices of Tibetan Esoteric Buddhism, and therefore possess exceptionally high scholarly value (Figure 1).

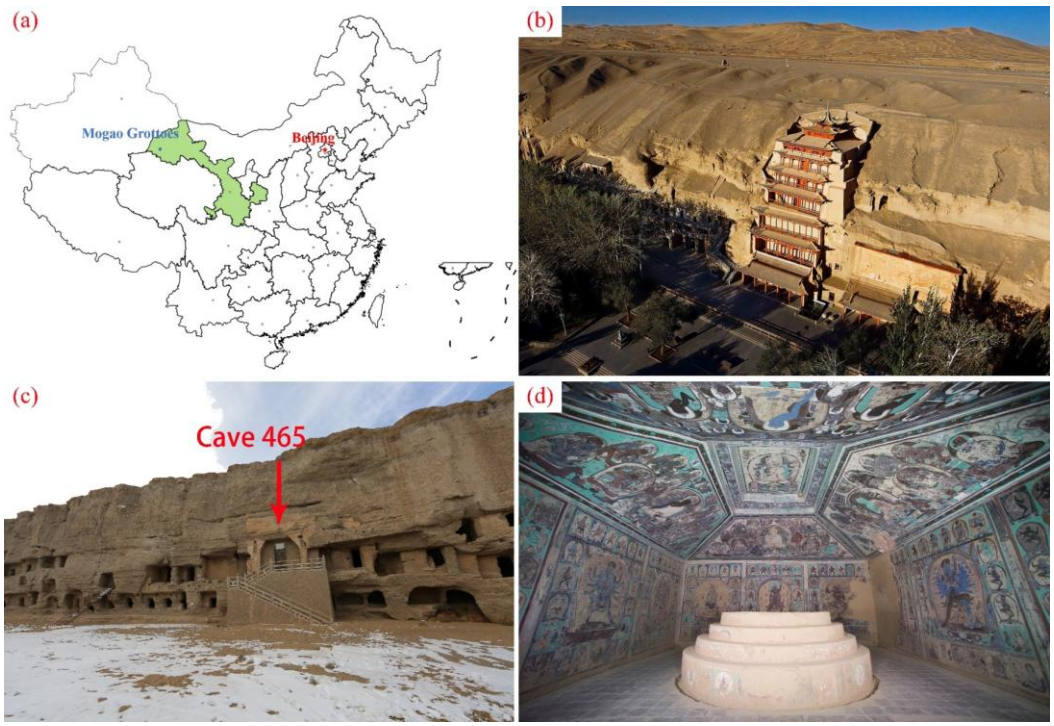


Figure 1. (**a**) Location map of the Mogao Caves. (**b**) Exterior view of the Mogao Caves. (**c**) Exterior view of Mogao Cave 465. (**d**) Interior view of the main chamber of Mogao Cave 465.

Scholarly research on Tibetan Buddhist painting has mainly focused on several aspects, including the history and iconographic studies of Tibetan Buddhist murals, thangkas, and Buddhist sculptures [2–7], with particular emphasis on the interpretation of thematic content, deity genealogies, and iconographic canons; studies on the history of Tibetan Buddhist painting styles [8], which have clarified the transmission and transformation of painting traditions across different regions and historical periods, as well as the influence of external cultures; studies of traditional Tibetan painting techniques [9,10], which have systematically documented the preparation of pigments, color mixing, and painting procedures employed by ancient artists and discussed the principles of color application and color matching; and analyses of the materials and techniques used in murals and thangkas [11–13] in which modern analytical techniques have been employed to characterize the material composition of pigments, preparatory layers, and binding media.

Existing studies of Mogao Cave 465 have predominantly focused on the humanities and social sciences, including archaeological investigations and chronological attribution [14–18], identification of mural imagery and interpretation of Esoteric Buddhist iconographic canons [19,20], interpretation of inscriptions within the cave [21], and analyses of artistic characteristics. Scientific studies, by contrast, have mainly addressed the spatial and temporal distribution of temperature and relative humidity in the cave [22], pigment identification and the reconstruction of faded inscriptions on the ceiling murals using

long-range hyperspectral imaging systems and self-developed algorithms [23], and the influence of multilayer mural painting techniques on conservation treatment [24].

In accordance with Buddhist iconometric principles and ritual canons, the mudras, postures, colours, identifiers and attributes (ritual implements) of Buddhist deities follow strict conventions. Colours and attributes in painted representations cannot be arbitrarily modified [25]. These features serve as the basis for scholars to identify iconographic figures. However, the murals in Cave 465 suffer from severe discolouration; most present colours appear black, grey or dark-toned, or mottled white, masking the original colour scheme and rendering them unsuitable for iconographic verification. When identifying Yab-yum images, Xie Jisheng stated that "owing to the extreme discolouration of the murals in this cave, we cannot determine the inherent colours of the depicted figures without interpretation from the perspective of Buddhist iconography" [19] (p. 3). Constrained by this issue, previous iconographic identifications of Cave 465 have relied solely on morphological features such as mudras, postures, ritual implements and associated mounts, with no supporting evidence from colour information.

To tackle this research limitation, the present study focuses on the Esoteric Buddhist murals of Mogao Cave 465. A combination of multiple analytical methods was adopted to characterise pigment compositions and examine colouring techniques. The original colours of the murals were inferred from experimental data, and these were further compared with the relevant iconographic prescriptions of previously identified deities and conventional colours used in thangkas to discuss their correlations. The results of this study provide colour evidence for the identification of deity figures in Cave 465, offer an important reference for research on Tantric Buddhist imagery in the Dunhuang grottoes, and supply a scientific basis for the colour reconstruction of Cave 465 murals.

2. Materials and Methods

The murals in Cave 465, as with other Mogao Grottoes murals, were executed using the secco technique. During preparation, a coarse plaster layer was first applied to the rock substrate, mixed from local Chengban clay (flood-deposited fine clay from Dunhuang), sand and wheat straw in a specific proportion. After drying, a fine plaster layer consisting of Chengban clay, sand and hemp fibre was laid over the coarse layer. When thoroughly dry, successive coats of white pigments (gypsum, calcite, kaolinite, muscovite, etc.) were applied to form the ground layer, before the deity images were painted on this surface. Animal glue is generally employed as the binding medium for the pigments, as reported in previous studies. This study focuses primarily on the constituent materials of the pigment layers and colouring techniques.

To investigate the painting materials and techniques of murals in Cave 465, 23 detection points were selected on the ceiling caisson, four sloped surfaces and four walls of the main chamber. These points cover a representative range of iconography, including Buddhas, various Vajra deities, their consorts, and protective deities.

2.1. Sample Collection and Preparation

In situ elemental analysis was first carried out at all 23 detection points using a portable Niton XL3t-800 X-ray fluorescence (XRF) spectrometer (Thermo Scientific, Billerica, MA, USA). Subsequently, micro-destructive sampling was performed at these locations following two sampling strategies.

The first type comprises fragment samples, which are prepared for cross-section embedding, stratigraphic observation, and scanning electron microscopy coupled with energy-dispersive X-ray spectroscopy (SEM-EDS) analysis to characterise elemental distributions across individual stratigraphic layers of pigment cross-sections. Fragments were collected exclusively from damaged mural areas, selected to be representative and to

preserve complete colour stratigraphy; the maximum dimension of each fragment did not exceed 2 mm × 2 mm, in strict accordance with the principle of minimal intervention.

The second type comprises powder samples, scraped carefully from damaged mural surfaces with a scalpel, and the total mass of each collected powder sample was limited to less than 1 mg. The powder samples are intended for X-ray diffraction (XRD), Raman spectroscopy and thermally assisted hydrolysis and methylation–pyrolysis–gas chromatography/mass spectrometry (THM-Py-GC/MS) analyses. XRD and Raman spectroscopy were combined to achieve reliable identification of pigment compositions, while THM-Py-GC/MS was used to verify the presence of organic colourants and identify the binding media.

The number of samples examined by each analytical method is shown as follows, with detailed sample information listed in Table 1: Raman spectroscopy on 20 samples, XRD on 10 samples, THM-Py-GC/MS on 2 samples, cross-section PLM imaging on 16 samples, and SEM-EDS on 4 samples. The micro-destructive sampling in this research was authorised by the Dunhuang Academy.

Table 1. Sample information for Cave 465.

Sample ID	Sampling Location	Surface Colour	Analytical Techniques
S01	Central Buddha, right shoulder, caisson ceiling	greyish-black	XRF, XRD, Raman, PLM, THM-Py-GC/MS
S02	Central Buddha, right shoulder, southern slope	blackish-brown	XRF, Raman, PLM, SEM-EDS
S03	Central Buddha, right shoulder, western slope	pale red	XRF, Raman, PLM, THM-Py-GC/MS
S04	Central Buddha, right shoulder, eastern slope	blue	XRF, XRD, Raman, PLM
S05	Central Buddha, right shoulder, northern slope	green	XRF, XRD, Raman, PLM
S06	Single deity, chest, southern panel, west wall	greyish-black	XRF, Raman
S07	Yab-yum figure, male deity`s right hand, central panel, west wall	purplish brown	XRF, XRD, Raman, PLM
S08	Yab-yum figure, consort`s right arm, central panel, west wall	reddish-brown	XRF, XRD, Raman
S09	Single deity, neck, northern panel, west wall	reddish-brown	XRF, PLM
S10	Yab-yum figure, male deity's right knee, eastern panel, south wall	blue	XRF, XRD
S11	Yab-yum figure, consort's abdomen, eastern panel, south wall	blackish-brown	XRF, XRD
S12	Yab-yum figure, male deity's right elbow, central panel, south wall	bluish-black	XRF, Raman, PLM, SEM-EDS
S13	Yab-yum figure, consort's left thigh, central panel, south wall	greyish-blue	XRF, Raman, PLM
S14	Yab-yum figure, male deity's right upper arm, western panel, south wall	bluish-black	XRF, Raman, PLM
S15	Yab-yum figure, consort's left upper arm, western panel, south wall	pink	XRF, XRD, Raman, PLM, SEM-EDS
S16	Yab-yum figure, male deity's face, central panel, north wall	blue	XRF, Raman, PLM
S17	Yab-yum figure, consort's ear, central panel, north wall	dark greyish-blue	XRF, Raman, PLM
S18	Single deity, left upper arm, eastern panel, north wall	reddish-brown pink	XRF, XRD, Raman
S19	Single deity (2nd from left), deity's right leg, upper eastern panel, north wall	black	XRF, Raman, PLM, SEM-EDS

S20	Single deity (3rd from left), deity's waist, upper eastern panel, north wall	pale red	XRF, XRD, Raman, PLM
S21	Single deity (5th from left), deity's right forearm, upper eastern panel, north wall	blue	XRF, Raman
S22	Single deity, deity's chest, upper area south of the doorway, east wall	greyish-white	XRF, Raman, PLM
S23	Single deity, deity's abdomen, lower-left area south of the doorway, east wall	reddish-brown	XRF, Raman

For stratigraphic examination of the pigment layers, cross-section specimens were prepared from the collected fragments. First, fragments were documented using a VHX-1000 digital microscope (Keyence, Osaka, Japan). Specimens were embedded in EpoThin™ 2 epoxy resin mixed with its curing agent at a mass ratio of 20:9 (Buehler, Lake Bluff, IL, USA). After thorough stirring, the mixture was vacuum-degassed to eliminate entrapped air bubbles. A two-step embedding procedure was adopted: half of the resin mixture was poured into the mould and cured, the fragment was positioned on the cured resin base, and the mould was then filled with the remaining resin. Once fully cured, the resin block was demoulded. Sequential grinding was performed on a MetaServ 250 grinder-polisher (Buehler, Lake Bluff, IL, USA) with silicon carbide abrasive papers of 240, 600 and 1200 grit. Grinding was followed by polishing: monocrystalline diamond suspensions of 6 μm and 1 μm were used for intermediate polishing, while 0.3 μm and 0.05 μm alumina (Al_2O_3) suspensions were applied for fine finishing on polishing cloths. Cross-section quality was inspected under polarised light microscopy (PLM); only surfaces free of scratches with clear stratigraphic features were selected for subsequent stratigraphic imaging and SEM-EDS examination.

2.2. Analytical Instruments

(1) X-ray fluorescence spectroscopy (XRF)

A portable Niton XL3t-800 X-ray fluorescence spectrometer (Thermo Scientific, Billerica, MA, USA) equipped with an Ag-anode X-ray tube (maximum rating of 50 kV, 40 μA), a high-resolution Si-PIN X-ray detector (resolution: 195 eV), and a 1 cm measurement spot was utilised for preliminary elemental characterisation of mural pigments. Data acquisition lasted 1 min, using the instrument's built-in mining mode. This pre-programmed quantitative routine adopts fundamental parameter algorithms, was originally calibrated for geological and mineral matrices, and is well suited to the analysis of mineral-based pigments. Measurements were carried out in air, with the detector window perpendicular to the pigment surface at a constant working distance and an 8 mm collimated beam. Factory fundamental-parameter calibration was used, with no additional empirical matrix correction. To reduce elemental interference from the underlying ground substrate, background spectra of the ground layer were acquired before pigment measurement for spectral subtraction.

(2) Digital microscopy

A KEYENCE VHX-1000 digital depth-of-field microscope (Keyence, Osaka, Japan) equipped with a VH-Z20R lens (magnification range: 20–200×) and integrated illumination was used to capture micrographs of mural pigment-layer samples.

(3) Polarized light microscopy (PLM)

The DM 2700P polarized light microscope (Leica, Wetzlar, Germany), fitted with a 10× eyepiece (FOV = 22–25 mm), 12 V/100 W halogen transmitted-reflected illumination and a DMC2900 CCD camera system, was utilised to capture photomicrographs showing the stratigraphy of sample cross-sections, as well as plane-polarised and cross-polarised images of dispersed-pigment mounts.

(4) X-ray diffraction (XRD)

X-ray diffraction (XRD) was performed on a Rigaku D/MAX 2500V diffractometer (Rigaku, Tokyo, Japan) equipped with a rotating Cu Kα_1 X-ray source. The operating voltage and current were set to 40 kV and 100 mA, respectively. A θ/2θ continuous scan mode was adopted. Scans were collected from 5° to 70° (2θ), with a step size of 0.02° and a scanning rate of 5.00 °/min. This technique was used for phase identification of pigment samples.

Phase identification was accomplished by matching acquired diffraction patterns against the ICDD PDF-4+ database. A phase assignment was considered valid when the principal diagnostic peaks showed consistent positions and relative intensities. Minor peak deviations were interpreted as lattice distortion, solid-solution effects or heterogeneous mixing, which are common for ancient mural pigments.

(5) Scanning electron microscopy–energy-dispersive X-ray spectroscopy (SEM-EDS)

Scanning electron microscopy coupled with energy-dispersive X-ray spectroscopy (SEM-EDS) was used to support stratigraphic observation and elemental characterisation, including spot analysis and area mapping to resolve the distribution of characteristic pigment elements. Specimens were sputter-coated with platinum using a JEOL JFC-1600 Auto Fine Coater (JEOL, Tokyo, Japan) at a current of 20 mA for 180 s prior to examination to alleviate charging effects. Secondary electron (SE) micrographs, EDS spot spectra and elemental maps were acquired at an accelerating voltage of 25 kV with a working distance of 10 mm. The dwell time for each area mapping acquisition was 600 s, and the spectrometer setting was adjusted to SS 60 during EDS data collection. Elemental analysis was performed using a Bruker XFlash Detector 760 silicon drift detector (SDD) energy-dispersive X-ray spectrometer (Bruker, Berlin, Germany).

(6) Raman spectroscopy

Raman spectroscopic measurements were performed on a HORIBA LabRAM Odyssey confocal Raman microscope (HORIBA, Kyoto, Japan) equipped with an 800 mm focal-length Czerny–Turner achromatic spectrograph and a SynapseEM EMCCD detector. A 600 gr/mm holographic grating and a 50× long-working-distance objective were adopted for data collection, covering a spectral range of 0–2000 cm^{-1}. Each laser source had a maximum output power of 100 mW. Neutral density (ND) filters were used to attenuate the laser and prevent thermal damage to mural pigments. Three excitation lasers with different ND filter settings were selected according to pigment types:

Red pigments: 785 nm excitation, 5% ND filter, acquisition time of 5 s per spectrum, 3 accumulations;

Yellow pigments: 633 nm excitation, 5% ND filter, acquisition time of 5 s per spectrum, 3 accumulations;

Blue, green and white pigments, as well as indigo (blue-black) and carbon black: 514 nm excitation, 3.2% ND filter, acquisition time of 5 s per spectrum, 3 accumulations.

Notably, 633 nm excitation also yields favourable spectral results for carbon black. The system was calibrated against a silicon reference standard (520.7 cm^{-1}) before each measurement session to correct Raman shift. All spectra were acquired and processed using LabSpec 6 software.

(7) Thermally assisted hydrolysis and methylation–pyrolysis–gas chromatography/mass spectrometry (THM-Py-GC/MS)

Organic pigments and binding materials were analyzed using an EGA/PY-3030D pyrolyzer (Frontier Laboratories, Koriyama, Japan) coupled to an Agilent 7890B-5977B gas chromatograph–mass spectrometer (Agilent Technologies, Santa Clara, CA, USA). An HP-5MS non-polar capillary column (30 m × 250 μm × 0.25 μm) was used for

chromatographic separation. For gas chromatography, the oven temperature was initially set at 45 °C, increased to 150 °C at a rate of 5 °C/min and held for 2 min, followed by an increase to 200 °C at 5 °C/min and a 5-min hold, and finally increased to 300 °C at 10 °C/min. Helium was used as the carrier gas at a flow rate of 1 mL/min, with a split ratio of 50:1. Mass spectrometric analysis was performed using an electron ionization source and a single-quadrupole mass analyzer. The ion source and quadrupole temperatures were maintained at 230 °C and 150 °C, respectively. Data were acquired in full-scan mode at a scan rate of 1 scan/s over an m/z range of 50–700. Compounds were identified using the NIST 07 database and the Getty Conservation Institute's RAdICAL database. For pyrolysis, approximately 0.2 mg of sample was mixed with 3 µL of 25% tetramethylammonium hydroxide (TMAH) aqueous solution and placed in a stainless-steel sample cup. The sample was then inserted into a dedicated quartz liner for analysis. The pyrolysis temperature was set at 600 °C with a pyrolysis time of 0.2 min. The temperatures of the injector and the interface connecting the pyrolyzer to the chromatograph were maintained at 300 °C [26,27].

3. Results and Discussion

3.1. Results of Materials Analysis

In situ non-destructive XRF analysis was conducted across 23 detection points. The results show that red, pink and some reddish-brown areas are characterised by dominant lead (Pb), mercury (Hg) and iron (Fe) signals, which suggest the presence of red lead, cinnabar and hematite. Since Fe and calcium (Ca) also originate from the plaster layer, complementary instrumental analysis is required to confirm hematite. The green area S4 shows dominant copper (Cu) signals, and further analysis using XRD or Raman is needed to distinguish between atacamite and malachite. Cu was also detected in blue areas S4, S10, S16 and S21, consistent with azurite. Blue-black areas S11 and S14 yielded Pb, Fe and Ca signals, indicating potential plattnerite, with no detectable blue chromogenic elements. Arsenic (As) was detected in blackish-brown S2, reddish-brown S9 and black S19, implying that orpiment or realgar may exist in the underlying layers. In addition, Ca and Fe are the main characteristic elements of the ground layer, pointing to gypsum or calcite.

Laboratory XRD and Raman results further confirmed the pigment composition. Red pigments include red lead, cinnabar and hematite; white pigments comprise gypsum, calcite, quartz, muscovite, kaolinite and albite; yellow pigments are orpiment and realgar; and the green pigment is atacamite. Discrepancies were observed between the two techniques: XRD identified atacamite and botallackite, whereas Raman detected atacamite and azurite. This difference arises from their sampling scales. Raman analyses were performed on micrometre-scale single points, which coincidentally intercepted particles of both atacamite and azurite. By contrast, XRD provides bulk average information from the whole powder aliquot and detected atacamite and botallackite. The low abundance of azurite falls below the detection limit of XRD. It is thus inferred that azurite may be a contaminant or originate from impure atacamite pigment. Botallackite is likely an alteration product of atacamite. Blue pigments include azurite and the organic pigment indigo, while carbon black and plattnerite were identified as black pigments.

THM-Py-GC/MS analyses of samples S1 and S3 are provided in Appendix A. The organic pigment indigo was identified in S1, while indigo and shellolic acid were detected in S3. Shellolic acid is only indicative of shellac resin, whereas this analytical method cannot detect laccaic acid, the marker for lac dye. Two scenarios are therefore proposed. First, only shellac resin exists without lac dye, yet published studies have not documented its sole use as a binding medium for mineral pigments or a surface coating on Mogao murals. Second, lac dye and shellac resin co-occur, and this coexistence can be rationalised by different traditional lac dye preparation routes: the conventional boiling process for pigment extraction

may leave residual shellac resin due to incomplete separation, while direct grinding of lac insects with glue yields material with higher shellolic acid content, and shellolic acid is present in products from both approaches. The authors favour this second scenario. Raman data for S3 also revealed cinnabar, but the red paint layer is thin and heterogeneously distributed. If shellac resin acted only as a surface coating, such thin, uneven cinnabar application would be less expected. We therefore hypothesise that lac dye was originally used as a pigment constituent, and its current appearance results from subsequent fading or colour alteration. In addition, animal glue was detected in both samples.

Microscopic observations of pigment cross-sections, together with XRF, XRD and Raman results, are summarised in Table 2. SEM-EDS results are provided in Appendices B–E. The pigment stratigraphy and elemental distribution will be discussed in the following section with reference to these deity images.

Table 2. Analytical results of mural samples from Cave 465.

Sample ID	XRF Elemental Results	XRD Phase Identification	Raman Phase Identification	Cross-Section Stratigraphic Observations
S01	Ca, Fe	Gypsum, Calcite, Quartz, Muscovite, Kaolinite, Albite	carbon black	Two pigment layers: the white underlayer (ca. 76 μm) and upper black layer (ca. 2.55 μm).
S02	As, Pb, Ca, Fe	/	orpiment, red lead, cinnabar	Two pigment layers: the mixed underlayer of yellow, white and minor red pigment grains (ca. 17.43 μm), and an extremely thin, discontinuous upper black layer (ca. 2.8 μm).
S03	Hg, Ca, Fe	/	cinnabar	Two pigment layers: the red underlayer (ca. 5.57 μm), and an extremely thin, discontinuous upper black layer.
S04	Cu, Fe, Ca	azurite, quartz	azurite, hematite	Two pigment layers: the red underlayer (ca. 9 μm), and an upper layer of blue pigment mixed with minor red pigment (ca. 26 μm).
S05	Cu, Ca, Fe	atacamite, botallackite, gypsum	atacamite, azurite	One pigment layer: uniform green (ca. 40 μm)
S06	Pb, Ca, Fe	/	indigo, plattnerite	/
S07	Pb, Cu, Ca, Fe	plattnerite, quartz	azurite, plattnerite	One pigment layer: uniform red (ca. 25–50 μm)
S08	Pb, Ca, Fe	plattnerite, quartz, muscovite, albite	red lead, plattnerite	/
S09	Pb, As, Ca, Fe	/	/	Two pigment layers: yellow underlayer, red overlayer; no sharp boundary and downward penetration of the red overlayer into the yellow underlayer
S10	Cu, Fe, Ca	azurite, quartz	/	/
S11	Pb, Ca, Fe	plattnerite, calcite, quartz, albite	/	/
S12	Pb, Ca, Fe	/	indigo, azurite, carbon	One pigment layer: mixed dark-blue, blue and white pigments (ca. 15 μm)
S13	Cu, Fe, Ca	/	azurite, hematite	One pigment layer: light-blue matrix with minor red pigment particles (ca. 60 μm)
S14	Pb, Ca, Fe	/	indigo	One pigment layer: dark-blue pigment grains and non-granular blue, both mixed with white matrix (ca. 14 μm)
S15	Hg, Pb, Ca, Fe	cinnabar, plattnerite, quartz, calcite	cinnabar, plattnerite	Two pigment layers: orange underlayer (ca. 3.4 μm) and deep-red overlayer (ca. 5 μm), upper red penetrating into the orange underlayer.
S16	Cu, Fe, Ca	/	azurite, hematite	One pigment layer: blue pigment with scattered red pigment grains (ca. 25 μm)

S17	Cu, Fe, Ca	/	azurite, hematite	Two pigment layers: the red underlayer (ca. 23 μm) and overlayer of blue containing scattered red pigment grains (ca. 20 μm); pigment grains in both layers are coarse.
S18	Pb, Hg, Ca, Fe	plattnerite, calcite, quartz, cinnabar	cinnabar, red lead, plattnerite	/
S19	Hg, As, Ca, Fe	/	realgar, orpiment, red lead	Three pigment layers: the white underlayer (ca. 40 μm), middle yellow layer (ca. 17 μm), and overlayer of black and orange (ca. 4 μm), with the orange component infiltrating downwards.
S20	Hg, Pb, Ca, Fe	plattnerite, calcite	cinnabar, red lead	One pigment layer: uniformly mixed red and orange pigments (ca. 16.5 μm)
S21	Cu, Fe, Ca	/	azurite, hematite	/
S22	Pb, Ca, Fe	/	indigo, azurite, gypsum	One pigment layer: mixture of dark-blue and white pigments (ca. 14 μm); the dark-blue component shows no distinct particulate texture.
S23	Pb, Fe, Ca,	/	plattnerite	/

3.2. Analysis of Pigment Application Techniques

3.2.1. Buddha Images on the Cave Ceiling

Five Buddha images are depicted at the centre of the ceiling caisson and the four sloped surfaces of the main chamber. Their present colour conditions are as follows: the central Buddha within the caisson exhibits a greyish-black tone, with patchy pigment spalling exposing the underlying white ground layer; the Buddha on the southern slope is reddish-brown, and its pigment layer is relatively well preserved; the Buddha on the western slope is pale red, and its thin paint layer allows the colour of the underlying white ground to show through; the Buddha on the eastern slope presents a vivid blue hue, with patchy reddish-brown areas; the Buddha on the northern slope is green with relatively homogeneous colouration.

Sample S01 was taken from the central Buddha in the caisson. PLM of the cross-section reveals two pigment layers: the white underlayer is relatively thick, approximately 76 μm. XRD identifies its constituents as gypsum, calcite, quartz, muscovite, kaolinite and albite. The overlayer is comparatively thin, around 2.5 μm. Raman spectroscopy detects carbon black, (Figure 2) while THM-Py-GC/MS confirms the organic colorant indigo (THM-Py-GC/MS data are provided in Appendix A). Combined with the visual tone of the mural, it is inferred that a white pigment was applied as the underlayer, over which a top layer of carbon black mixed with indigo was glazed. This technique of blending indigo with carbon black to modify the visual effect is known in traditional Chinese painting.

Sample S02 was collected from the central Buddha on the southern slope. PLM observation of the cross-section shows two pigment layers. The underlayer consists of a mixture of yellow, white and minor red pigments, with a thickness of approximately 17.4 μm. The overlayer is an extremely thin, discontinuous black pigment layer, around 2.8 μm thick. Raman spectroscopy on the powder sample identifies orpiment, red lead and cinnabar; red lead is also detected in dark purple pigment particles (Figure 3). No diagnostic signal has yet been obtained for the black particles. SEM-EDS results reveal that the red particles within the underlayer contain Pb, which are presumed to be red lead. Elemental mapping indicates that the pigment layer is dominated by Pb, As and S, while Hg is not detected (detailed SEM-EDS results are listed in Appendix B). It is therefore inferred that the underlayer was mainly painted with orpiment mixed with a small amount of red lead and white pigment. The cinnabar detected by Raman may represent impurities introduced during painting. The black particles may be surface contamination or plattnerite; restoration materials may also interfere with the Raman signals acquired from the overlayer. Considering the principles of colour mixing, this blend would be expected to yield a pale orange-yellow

hue. The current reddish-brown tone is most probably caused by the darkening of red lead, corresponding to the purple pigment particles identified in the Raman spectra.

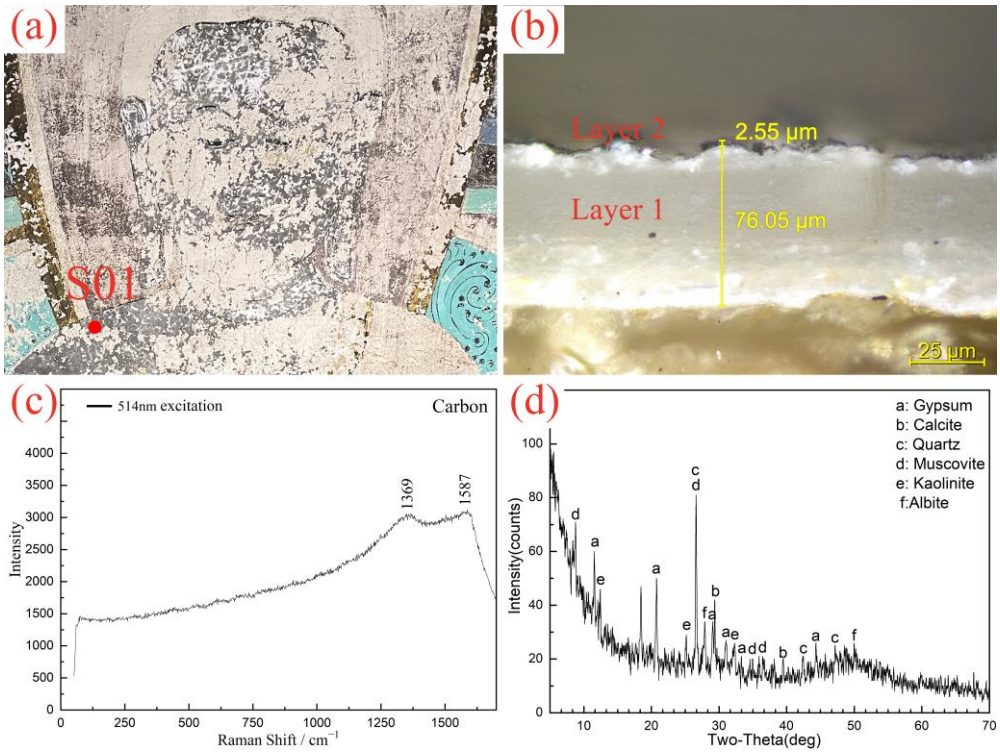


Figure 2. (**a**) The central Buddha on the caisson ceiling; (**b**) photomicrograph of the pigment cross-section (500×); (**c**) Raman spectrum; (**d**) XRD pattern.

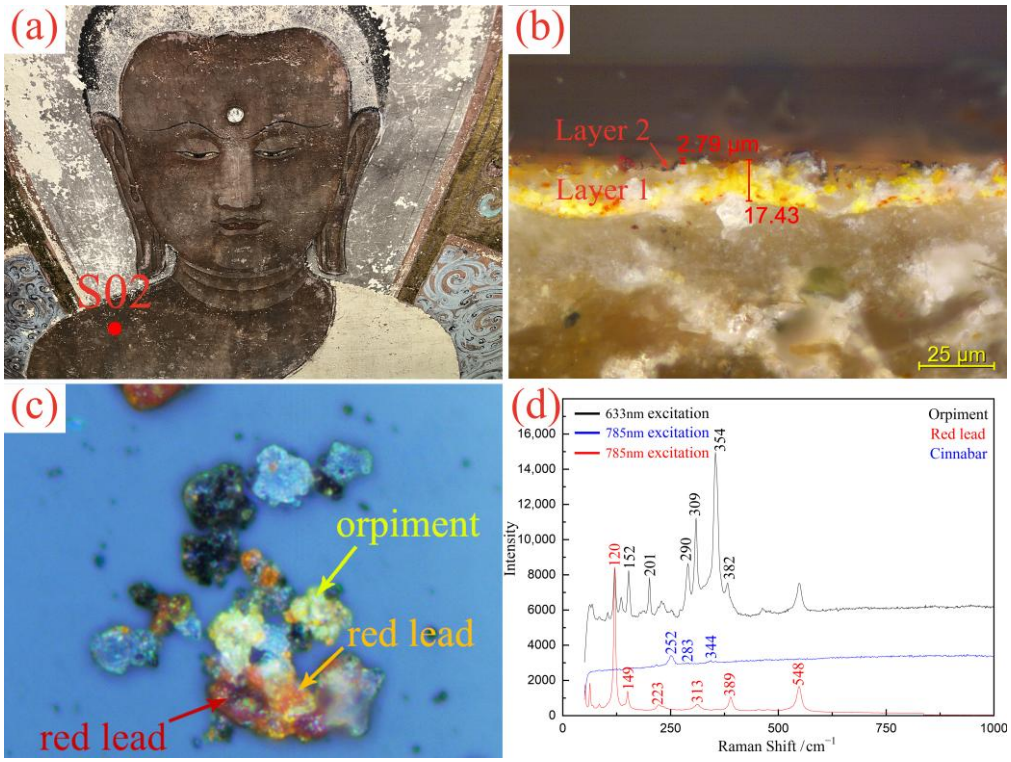


Figure 3. (**a**) The central Buddha on the southern slope; (**b**) photomicrograph of the pigment cross-section (500×); (**c**) micrograph of pigment particles under a Raman microscope (50×); (**d**) Raman spectra.

Sample S03 was collected from the central Buddha on the western slope. PLM observation of the cross-section reveals two pigment layers. The underlayer is red, with a thickness of approximately 5.57 μm. The overlayer consists of an extremely thin, discontinuous black layer. Raman spectroscopy identifies the red pigment as cinnabar (Figure 4), and no diagnostic signal was obtained for the black particles in the overlayer. THM-Py-GC/MS detected indigo and shellolic acid. The red pigment layer is homogeneous in cross-section and lacks a surface protective coating. Considering the visual colour effect of the mural, it is inferred that this area was painted using lac dye mixed with a small amount of cinnabar. The indigo signal may arise either from impurities incorporated during paint preparation or application, or from exogenous contamination introduced during sampling, or it may be associated with the thin black particles on the surface.

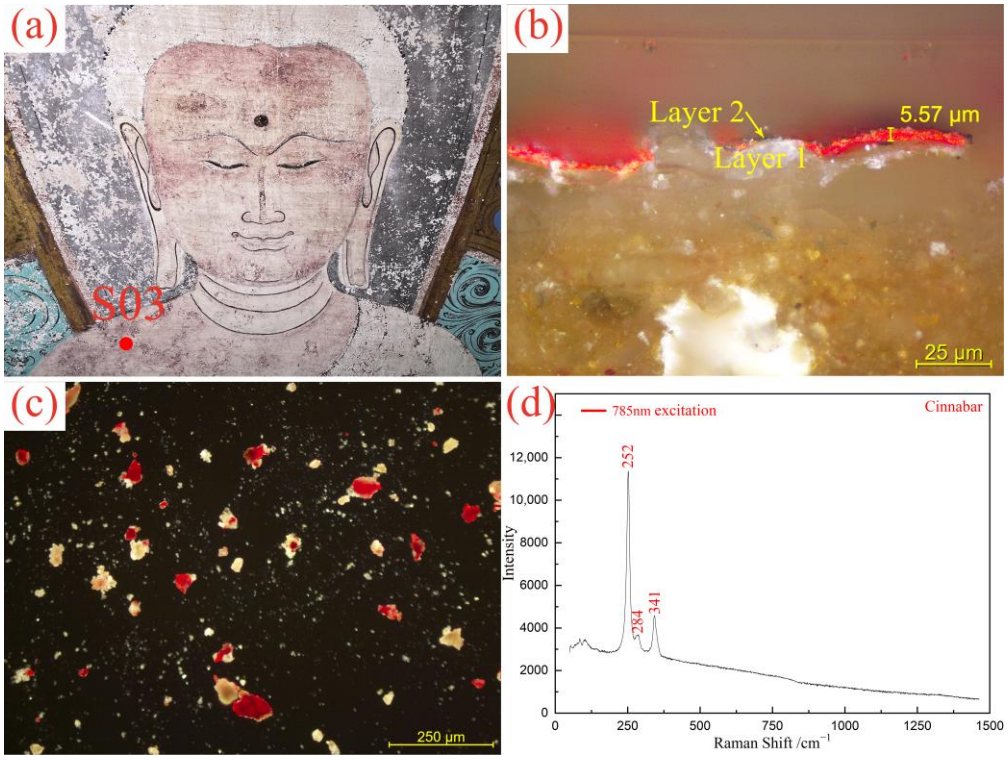


Figure 4. (**a**) The central Buddha on the western slope; (**b**) photomicrograph of the pigment cross-section (500×); (**c**) photomicrograph of pigment grains (100×, XPL); (**d**) Raman spectrum.

Sample S04 was collected from the central Buddha on the eastern slope. PLM observation of the cross-section reveals two pigment layers. The underlayer is dark red, with a thickness of approximately 9 μm. The overlayer consists of blue pigment mixed with minor red pigment, around 26 μm thick. Raman spectroscopy identifies the blue component as azurite and the red component as hematite. XRD only detects azurite (Figure 5). Based on previous analytical experience, XRD exhibits low sensitivity to trace amounts of hematite. It is reasonable to infer that hematite was applied as the underlayer, and azurite was overlaid on top during painting. The hematite particles observed within the azurite layer may have been picked up from the underlayer by the brush during application.

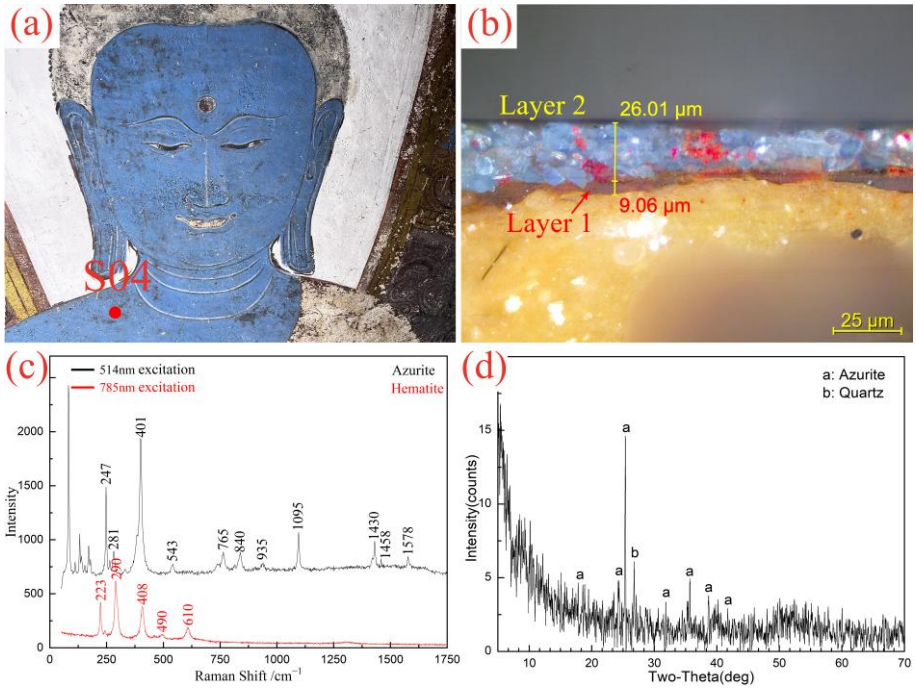


Figure 5. (**a**) The central Buddha on the eastern slope; (**b**) photomicrograph of the pigment cross-section (500×); (**c**) Raman spectra; (**d**) XRD pattern.

Sample S05 was collected from the central Buddha on the northern slope. PLM observation of the cross-section reveals a single, homogeneous green pigment layer with a thickness of approximately 40 μm. Both Raman spectroscopy and XRD identify the pigment as atacamite (Figure 6). The interpretations of azurite and botallackite detected by Raman and XRD, respectively, have been discussed in Section 3.1 and will not be repeated here. Evidently, the green area was painted in a relatively straightforward manner using only atacamite for flat colour application.

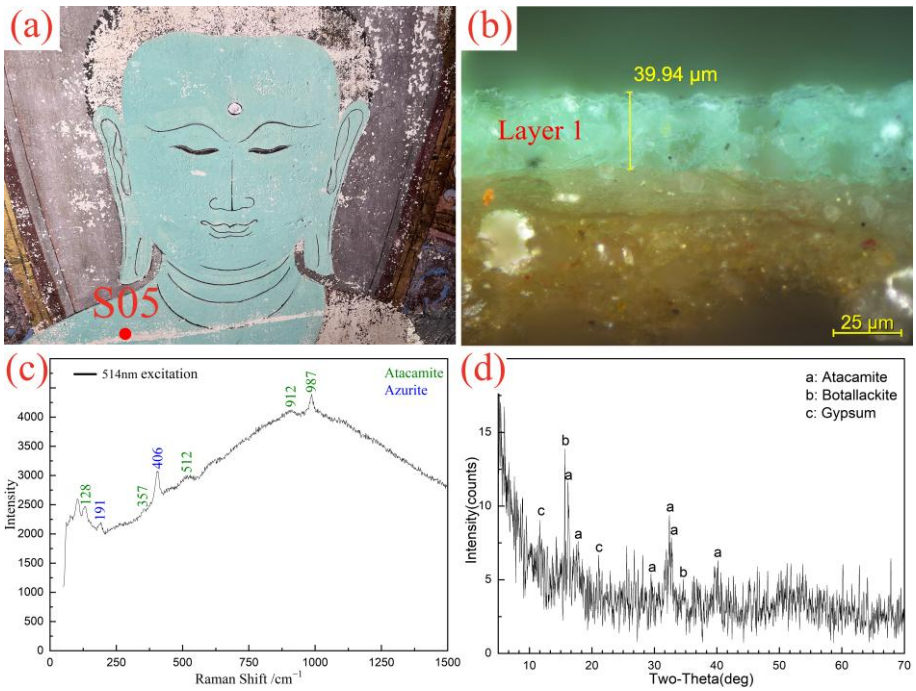


Figure 6. (**a**) The central Buddha on the northern slope; (**b**) photomicrograph of the pigment cross-section (500×); (**c**) Raman spectrum; (**d**) XRD pattern.

Scholars have identified the five Buddha figures described above as the Five Dhyāni Buddhas of Tibetan Buddhism. According to textual records, Vairocana occupies the central position and is white, embodying the wisdom of the Dharmadhātu; Akṣobhya is situated in the east and is blue, embodying the mirror-like wisdom; Ratnasambhava is located in the south and is golden yellow, embodying the wisdom of equality; Amitābha is in the west and is red, embodying the discriminating wisdom; Amoghasiddhi is in the north and is green, embodying the all-accomplishing wisdom [28]. Comparison indicates that the colours and orientations of the Buddha images on the western, eastern and northern slopes of Cave 465 are consistent with the iconographic prescriptions for the Five Dhyāni Buddhas. The Buddha on the southern slope currently exhibits a reddish-brown hue, and its original colour is inferred to have been pale orange-yellow, which resembles the golden yellow assigned to Ratnasambhava of the southern direction. The only point of divergence is the Buddha at the centre of the caisson: in Cave 465 it appears greyish-black, which is inconsistent with the white Vairocana described in textual sources. We surmise that, as the caisson represents the highest and most central space in the cave, a dark colour may achieve a more prominent visual effect than white.

3.2.2. Deity Images on the Western Wall

Three panels of deity figures are painted on the western wall of the main chamber. The central panel depicts a yab-yum figure. The male deity exhibits a complex colouration, with a greyish-purple tone overlying a reddish-brown base, and the overall hue approximates purplish-brown. The body of the female consort is reddish-brown. One single-deity panel is located on each of the southern and northern sides. The southern panel shows a male solitary figure with a greyish-black body; its pigment layer is flaking and patchy, revealing the underlying plaster layer. The northern panel features a female solitary figure, whose body is reddish-brown with a slightly warmer tone than that of the female consort in the central panel.

Sample S06 was collected from the male solitary figure in the southern panel. During Raman analysis, pigment grains were observable under the Raman microscope; fine reddish-brown particles were scattered on the surface of the blue-black pigment. Raman spectroscopy identifies the blue-black pigment as indigo and the reddish-brown particles as plattnerite (Figure 7). Since red and blue are generally complementary colours and are not ordinarily mixed for toning, two possible painting sequences are proposed for this area: one in which a red lead layer was first applied, followed by glazing with indigo; and another in which indigo was laid down first, with red lead subsequently used for surface washes. Both scenarios are plausible. Traditional Chinese painting includes practices involving mineral pigments as underlayers overlaid by transparent vegetable colour glazes. In addition, the supernatant of red lead pigment suspension, rather than its coarse sediment, was historically taken for skin washes on figures.

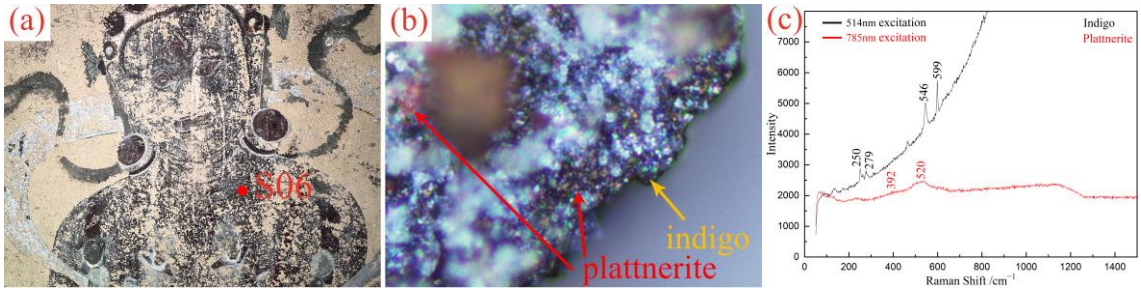


Figure 7. (**a**) The male solitary figure on the southern panel of the western wall; (**b**) micrograph of pigment particles under a Raman microscope (50×); (**c**) Raman spectra.

Sample S07 was taken from the male deity of the central yab-yum figure. PLM of the cross-section reveals a single red pigment layer approximately 25–50 μm thick. XRD detects plattnerite, while Raman spectroscopy identifies both plattnerite and azurite (Figure 8). Combined with the visual evidence of the mural, it is hypothesised that plattnerite forms the underlayer and azurite occurs as a thin overlying layer. Azurite was not detected by XRD owing to its low abundance, and its extreme thinness renders it susceptible to removal during grinding of the block specimen. If this stratigraphic interpretation is correct, the original colour scheme prior to the alteration of red lead can be reconstructed: a red base layer overlaid by a uniform blue glaze.

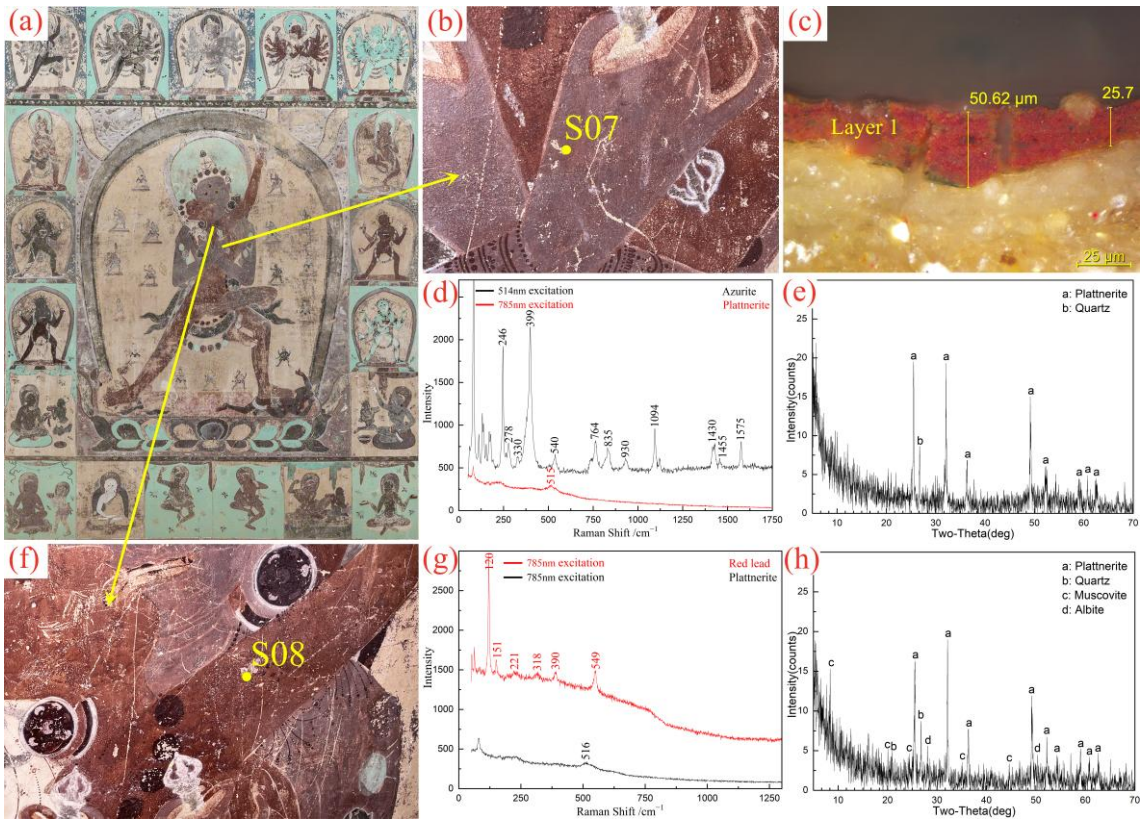


Figure 8. (**a**) Central yab-yum panel on the western wall; (**b**) right hand of the male deity; (**c**) photomicrograph of the pigment cross-section (500×); (**d**) Raman spectra of S7; (**e**) XRD pattern of S7; (**f**) right arm of the female consort; (**g**) Raman spectra of S8; (**h**) XRD pattern of S8.

Sample S08 was collected from the female consort. Raman analysis identifies red lead and plattnerite, and XRD detects plattnerite together with components of the ground layer. On this basis, it is reasonably inferred that this figure was painted solely with red lead applied as a flat wash; plattnerite formed subsequently via surface oxidation of the red lead pigment over time.

Sample S09 was collected from the female solitary figure in the northern panel. PLM examination of the cross-section reveals two pigment layers: a yellow underlayer and an overlying red layer, with no sharp boundary and downward penetration of the red overlayer into the yellow underlayer. The total pigment thickness is ca. 14 μm. XRF detects Pb and As. (Figure 9) Combined with previous analytical results, it is inferred that orpiment served as the underlayer, overlaid by red lead, whose surface has oxidised to plattnerite. If this interpretation is correct, the original appearance before discolouration would have been a warm orange hue produced by yellow orpiment as the base overlaid with red lead.

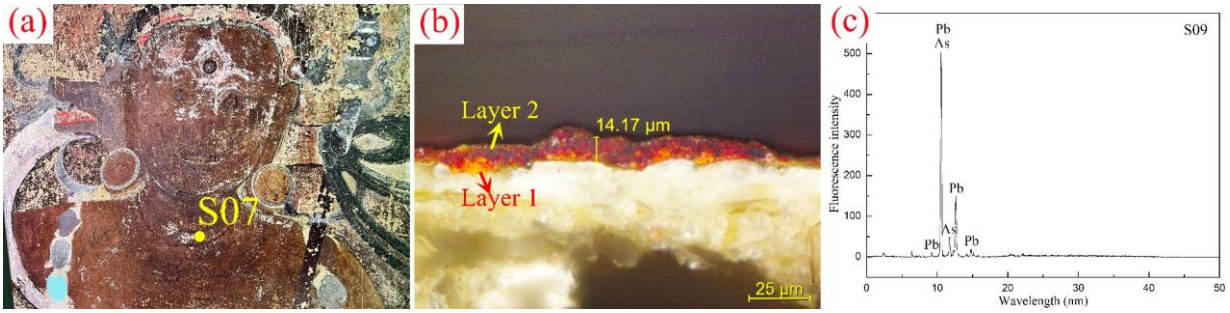


Figure 9. (**a**) The female solitary figure on the northern panel of the western wall; (**b**) photomicrograph of the pigment cross-section (500×); (**c**) fluorescence spectrum.

On the basis of iconographic features including the figure's form, head ornaments, attributes and posture, scholars identify the central yab-yum figure on this wall as Cakrasaṃvara and his consort Vajravārāhī, while the northern and southern panels depict the solitary forms of Cakrasaṃvara and Vajravārāhī, respectively. According to the iconographic prescriptions for the Cakrasaṃvara maṇḍala, Cakrasaṃvara is dark blue and Vajravārāhī is red [19]. In addition, in some Tibetan Buddhist thangkas, Cakrasaṃvara is shown in blue-black, symbolising space and primordial wisdom, and his consort Vajravārāhī is red, symbolising bliss and compassionate magnetism [29]. Comparison shows that the body colours of the female consort in the central yab-yum panel and the female solitary figure on the northern panel are consistent with the hues recorded in textual sources and commonly adopted in thangkas. For the male deity of the central yab-yum figure, however, our stratigraphic interpretation suggests an original colour scheme of red lead underlayer thinly glazed with azurite, which would yield a purplish-red composite tone. The male solitary figure on the southern panel is inferred to have been painted with superimposed red lead and indigo, likely producing a purplish-red or purplish-brown colour. This tone is close to that of the central male deity, yet diverges from the prescribed colour of Cakrasaṃvara in textual records.

3.2.3. Deity Images on the Southern Wall

Three yab-yum panels are painted on the southern wall of the main chamber. In the eastern panel, the male deity is blue, while the female consort is blackish-brown, overlaid by a very thin white layer on the upper torso. In the central panel, the male deity is bluish-black and the female consort is greyish-blue, with patchy reddish-brown areas in local regions. In the western panel, the male deity is bluish-black; the pigment is patchy and exfoliated, revealing the underlying ground layer. The female consort is pink, though extensive exfoliation gives her an overall pale appearance.

Sample S10 was taken from the male deity of the eastern yab-yum figure. XRD identifies azurite. Sample S11 was collected from the female consort. XRD detects plattnerite, together with calcite, quartz and albite from the ground layer (Figure 10). No signal was obtained for the overlying white substance. The analytical results show that the reddish-brown body colour is plattnerite. It is hypothesised that the figure was originally painted with red lead, which darkened upon oxidation over time. Since no further analysis was performed on the superficial white layer, we tentatively speculate, based on mural visual evidence and results from comparable detection points, that this white material may be a thin wash of azurite. In either scenario, this locally restricted, extremely thin layer is unlikely to alter the dominant body hue. We therefore surmise that the original body colour was red.

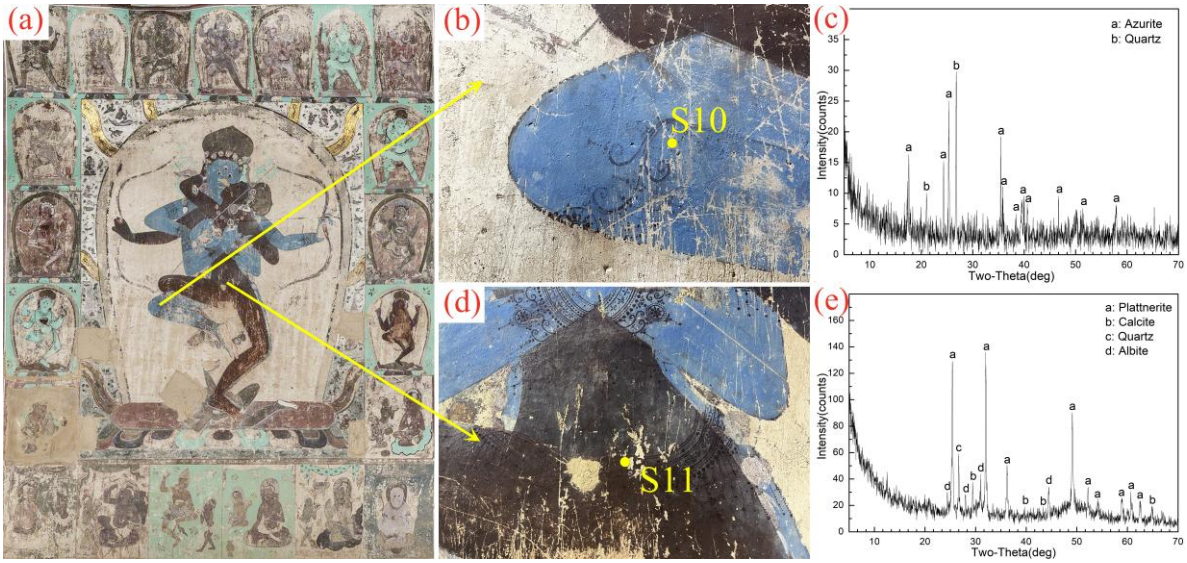


Figure 10. (**a**) Eastern yab-yum panel on the southern wall; (**b**) right knee of the male deity; (**c**) XRD pattern of S10; (**d**) waist of the female consort; (**e**) XRD pattern of S11.

Sample S12 was taken from the male deity of the central yab-yum figure. PLM of the cross section reveals a single pigment layer composed of dark blue, blue and white constituents, approximately 15 μm thick. Raman spectroscopy identifies indigo, azurite and carbon black. (Figure 11) SEM-EDS detects high Pb concentrations in the upper portion of the pigment layer, whereas Ca dominates the lower portion. Elemental mapping clearly shows abundant Pb distributed within the upper half of the pigment layer, and Cu is not detected (detailed SEM-EDS results are listed in Appendix C). Combined with XRF results of Pb, Fe and Ca, it is hypothesised that the azurite identified by Raman may represent an impurity introduced during painting. We therefore infer that this area was originally painted as a flat wash using indigo mixed with small amounts of white pigment and carbon black, followed by either a thin glaze or a local wash of red lead. If red lead was only applied as a local wash, the dominant overall tone would remain dark blue. If red lead was applied as a full surface glaze, the resultant colour might shift toward redder hues, potentially yielding a deep blue-purple tone. Nevertheless, based on cross-sectional observations and the absence of distinct lead-bearing pigment particles in the Raman spectra, we surmise that red lead was present in low quantities with fine particle sizes. Accordingly, the red hue contributed by red lead may not substantially alter the dark blue underlayer.

Sample S13 was collected from the female consort. PLM of the cross-section reveals a single relatively thick pigment layer (ca. 60 μm), consisting of blue pigment mixed with minor red grains. Raman spectroscopy confirms the blue component as azurite and the red component as hematite (Figure 11). It is inferred that the greyish-blue colour at the sampled location was produced by azurite blended with a small quantity of hematite. The stratigraphic relationship for the reddish-brown areas visible on the mural cannot be determined, as no cross-section sample was taken from these regions.

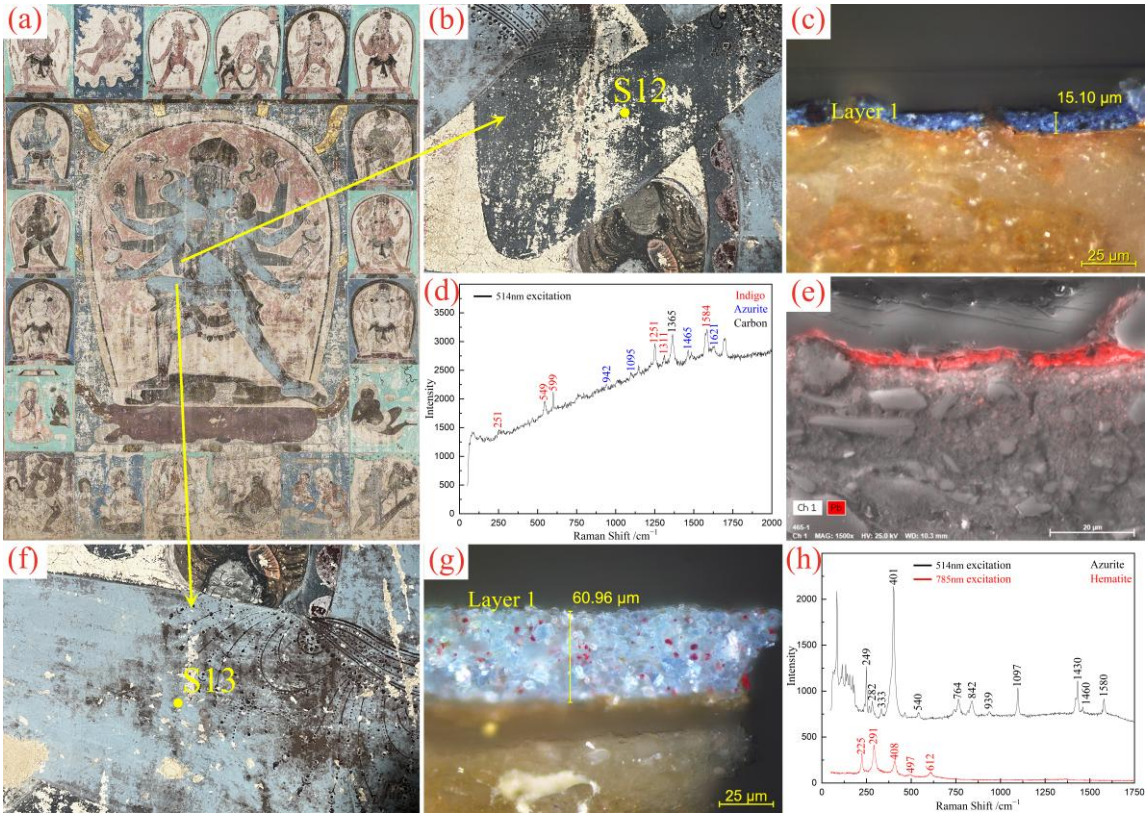


Figure 11. (**a**) Central yab-yum panel on the southern wall; (**b**) right elbow of the male deity; (**c**) photomicrograph of the pigment cross-section of S12 (500×); (**d**) Raman spectrum of S12; (**e**) EDS elemental map showing Pb distribution for the cross-section of S12; (**f**) left thigh of the female consort; (**g**) photomicrograph of the pigment cross-section of S13 (500×); (**h**) Raman spectra of S13.

Sample S14 was taken from the male deity of the western yab-yum figure. PLM of the cross-section reveals a single pigment layer composed of dark blue, blue and white constituents, approximately 14 μm thick. Raman spectroscopy identifies indigo, and XRF detects characteristic elements including Pb, Fe and Ca (Figure 12). This sample is highly similar to S6 and S12, suggesting identical painting materials and application methods; therefore, the details are not repeated here.

Sample S15 was collected from the female consort. PLM of the cross-section shows two pigment layers: an orange underlayer (ca. 3.5 μm) and an overlying deep red layer (ca. 5.1 μm). Raman spectroscopy identifies cinnabar and plattnerite, and XRD also detects cinnabar and plattnerite together with calcite and quartz from the ground layer (Figure 12). EDS elemental mapping clearly demonstrates that Pb is concentrated mainly in the upper layer, while Hg is concentrated in the underlayer (detailed SEM-EDS results are listed in Appendix E). It is therefore inferred that this region was painted with a flat wash of cinnabar as the base, followed by a thin glaze of red lead. Given the minimal thickness of both pigment layers, the superimposed colours would originally have produced a warm pink hue. Subsequent darkening caused by oxidation of the surface red lead transformed the original warm pink into the current cool, purplish-pink tone. Although both red lead and cinnabar are red pigments, cross-sectional observation reveals that the red pigment layer is less than 10 μm thick. Combined with visual evidence from the mural, this thin red layer allows the underlying white ground layer to show through, lightening the overall hue to pink.

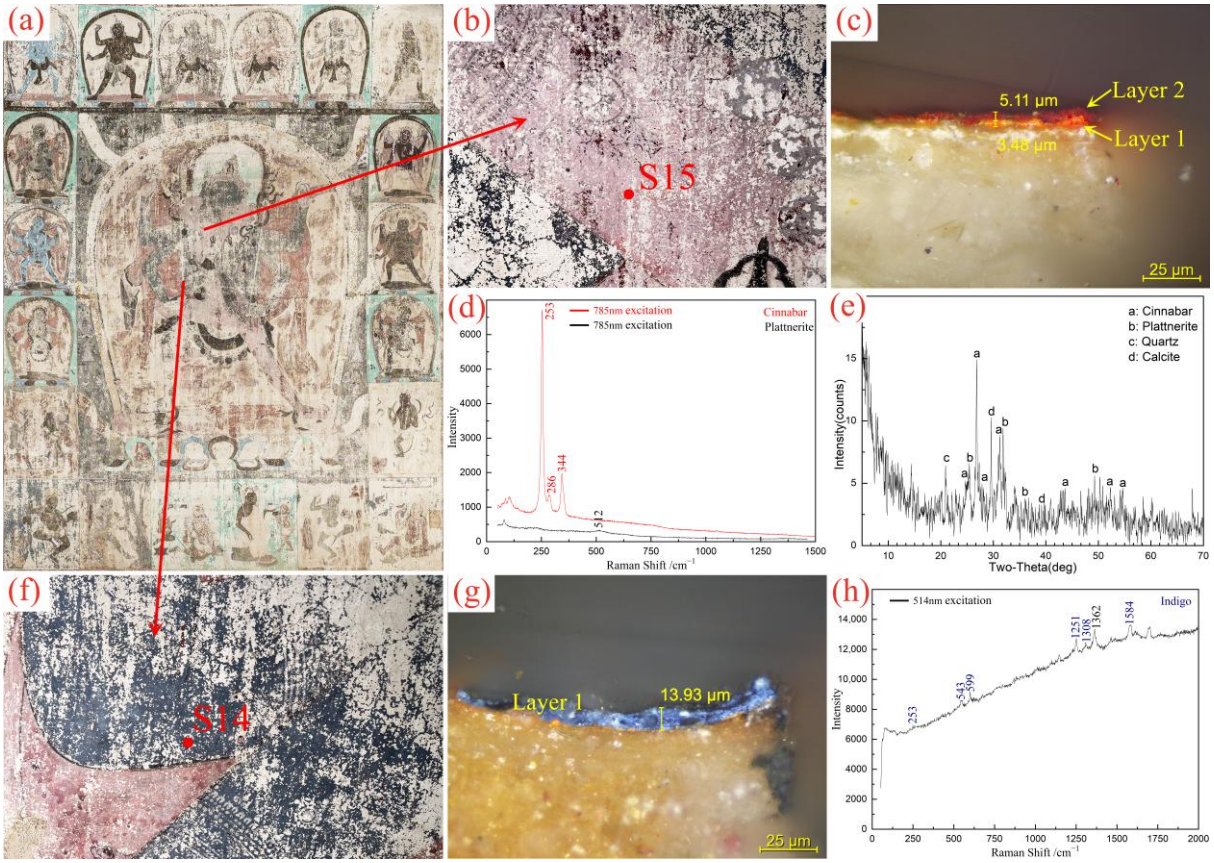


Figure 12. (**a**) Western yab-yum panel on the southern wall; (**b**) left upper arm of the female consort; (**c**) photomicrograph of the pigment cross-section of S15; (**d**) Raman spectra of S15; (**e**) XRD pattern of S15; (**f**) right upper arm of the male deity; (**g**) photomicrograph of the pigment cross-section of S14; (**h**) Raman spectrum of S14.

Scholars identify the eastern yab-yum figure as Mahāmāyā Vajra and Buddhāḍākinī, the central yab-yum figure as Guhyasamāja Vajra and Sparśavajrā, and tentatively assign the western yab-yum figure to Mahābala and his consort Cakravegā, based on iconographic features including form, head ornaments, attributes and posture recorded in the iconographic prescriptions. According to textual prescriptions, the wrathful Mahāmāyā Vajra has a blue body and his consort is red, with attributes consistent with those of Mahāmāyā Vajra [2,30]. Mahābala is described as dark blue/blackish-blue, with three faces, six arms, a skull crown surmounted by an emanating Buddha; his consort Cakravegā is usually red, with two arms and no independent attributes [4,30]. Although textual sources do not specify the body colours of the Guhyasamāja yab-yum figure, Guhyasamāja Vajra is commonly depicted in blue in thangkas, signifying his status as a Vajra deity. His consort is also blue, with three faces, six arms and two feet, and her crown, ornaments and all fine details mirror those of the main deity [29]. Comparison shows that the eastern yab-yum panel on the southern wall of Cave 465 aligns well with textual records: the male deity is blue, and the female consort is inferred to have been red before discolouration. The female consort in the central panel is blue, as is common in thangkas, though the manifestation of this blue differs slightly. Based on the inferences above, the small amount of red lead in the superficial layer of the male deities in the central and western panels may not substantially affect the dark blue underlayer. Thus, their overall colour would be dark blue, which is highly similar to the hues prescribed in textual sources and commonly seen for such deities in thangkas. Furthermore, the female consort in the western panel is inferred to have originally been pink; this pale tone arises because the red pigment layer is thin, revealing the underlying white ground layer, which differs slightly from the red colour specified in textual sources.

3.2.4. Deity Images on the Northern Wall

Two panels survive on the northern wall of the main chamber. The central panel depicts a yab-yum figure: the male deity is vivid blue, while the female consort shows a complex colour scheme, with a reddish-brown main colour and local greyish-blue on the surface. The eastern panel is a single deity, whose colouration differs from the other figures. It is painted in two colours: the right side of the deity's body is white with patchy reddish-brown exposed in places, and the left side is reddish-brown with patchy pink in local areas.

Sample S16 was taken from the male deity of the central yab-yum figure. PLM of the cross-section reveals a single pigment layer consisting of blue pigment mixed with minor red grains, approximately 25 μm thick. XRF detects Cu and Fe as characteristic elements. Raman spectroscopy confirms the blue component as azurite and the red component as hematite. (Figure 13) Combined with the visual features of the mural, it is inferred that this area was painted using azurite blended with a small amount of hematite, or alternatively, the hematite grains represent impurities incorporated during painting.

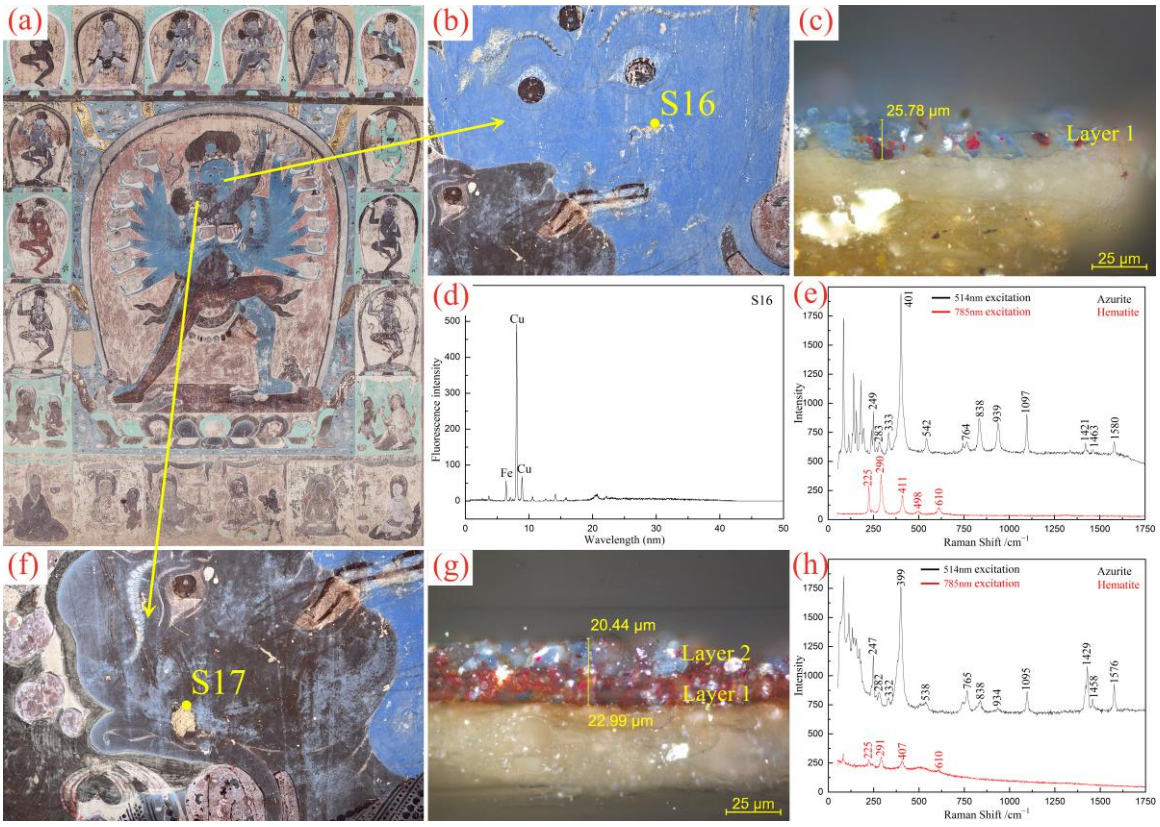


Figure 13. (**a**) Central yab-yum panel on the northern wall; (**b**) face of the male deity; (**c**) photomicrograph of the pigment cross-section of S16 (500×); (**d**) XRF spectrum of S16; (**e**) Raman spectra of S16; (**f**) ear of the female consort; (**g**) photomicrograph of the pigment cross-section of S17 (500×); (**h**) Raman spectra of S17.

Sample S17 was collected from the female consort. PLM of the cross section shows two pigment layers: a deep red underlayer (ca. 23 μm) and an overlying blue layer (ca. 20 μm). Red pigment grains from the underlayer are observed within the upper layer. This is interpreted as the brush lifting the underlying red pigment during the application of the top blue layer. Raman spectroscopy identifies azurite for the blue fraction and hematite for the red fraction. (Figure 13) It is hypothesised that this region was first painted with a flat wash of hematite as the base, followed by a wash of azurite. Considering the visual appearance of the mural, this superimposed colouring method produces an overall dark grey-blue effect.

Sample S18 was taken from the single deity of the eastern panel. Raman spectroscopy identifies cinnabar, red lead and plattnerite. Two subsamples, from the reddish-brown and pink regions respectively, were analysed by XRD. The results show that the reddish-brown subsample contains plattnerite, along with calcite and quartz from the ground layer, whereas the pink subsample contains cinnabar (Figure 14). Based on visual observation of the mural, it is hypothesised that this single deity was painted with a flat wash of red lead as the base. White pigment was then overlaid on the right side of the body, and cinnabar was applied as a wash on the left side. Accordingly, the original colour scheme is tentatively interpreted as pale pinkish-white on the right and red on the left.

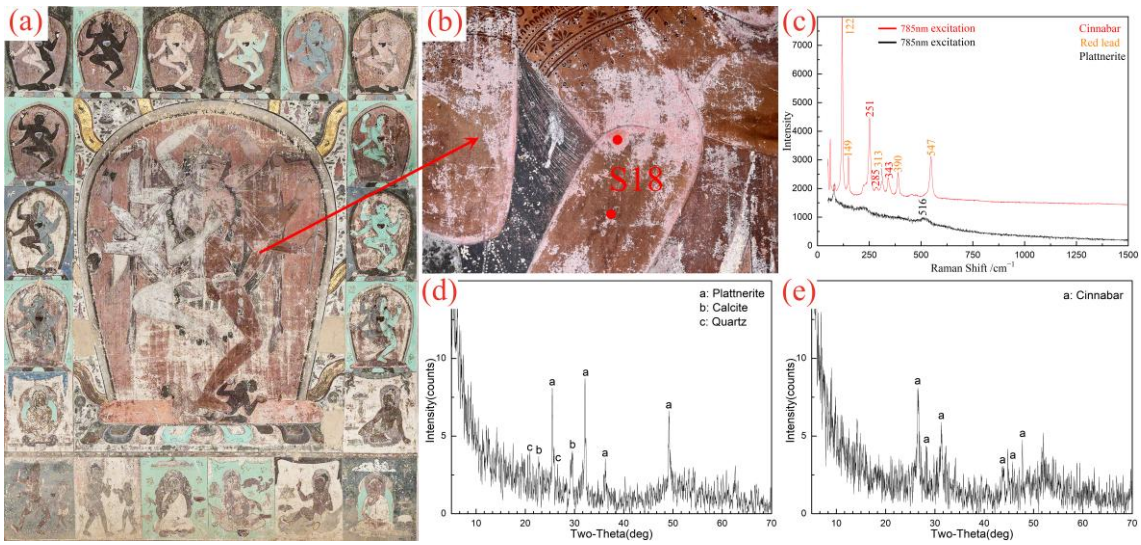


Figure 14. (**a**) Single deity panel on the eastern part of the northern wall; (**b**) left upper arm of the single deity; (**c**) Raman spectra of S18; (**d**) XRD pattern of the reddish-brown subsample of S18; (**e**) XRD pattern of the pink subsample of S18.

Scholars identify the central yab-yum figure on this wall as Hevajra and his consort Nairātmyā on the basis of the Tibetan Buddhist text *Hevajra Tantra*, which sets out the iconographic prescriptions for Hevajra [31] Hevajra is described as having eight faces and sixteen arms, with a blue body. The *Niṣpannayogāvalī* records that the consort Nairātmyā has a dark blue body [32]; furthermore, dark blue or bluish-black is also the common colour for Nairātmyā in thangka paintings [29]. Comparison shows that the blue colour of the male deity in Cave 465 is consistent with textual descriptions. The female consort was painted using superimposed pigments: a deep red hematite base layer was overlaid with azurite glazing, producing an overall dark grey-blue appearance. This hue bears some resemblance to the dark blue recorded in the *Niṣpannayogāvalī* and the conventional colour seen in thangkas, although we surmise there are some differences in colour presentation.

In addition, twelve small animal-headed figures are painted on both sides and above the single deity of the eastern panel on the northern wall. Four profile figures at the centre of the upper zone are rendered in black, pink, green and blue respectively. Four frontal figures on the left and right sides also adopt these four colours. The remaining four figures have bicoloured bodies, each composed of two of the four colours: pink–black, black–blue, blue–green, and green–reddish-brown.

Sample S19 was taken from the right knee of the second black figure counting from the left in the upper zone. PLM of the cross-section reveals three pigment layers: a white underlayer (ca. 40 μm), a yellow middle layer (ca. 17 μm), and an upper mixed black and orange layer (ca. 3.7 μm). Raman spectroscopy identifies orpiment and realgar as the yellow pigment grains, carbon black as the black grains, red lead as the brown grains, and cinnabar as the red grains within the powder sample. (Figure 15) SEM-EDS results show

that As is distributed throughout the pigment layers, while Hg is concentrated mainly in the uppermost layer (detailed SEM-EDS results are listed in Appendix E); Pb was not detected. The red lead identified by Raman may therefore represent incidental impurities. Combining the cross-section micrographs and EDS results, it is hypothesised that this area was prepared with a white ground layer, followed by a flat wash of orpiment-realgar paragenetic mineral pigment, and finally overlaid by glazing or local washing with cinnabar and carbon black. If this interpretation is correct, the superimposed colours would originally have produced a deep orange hue.

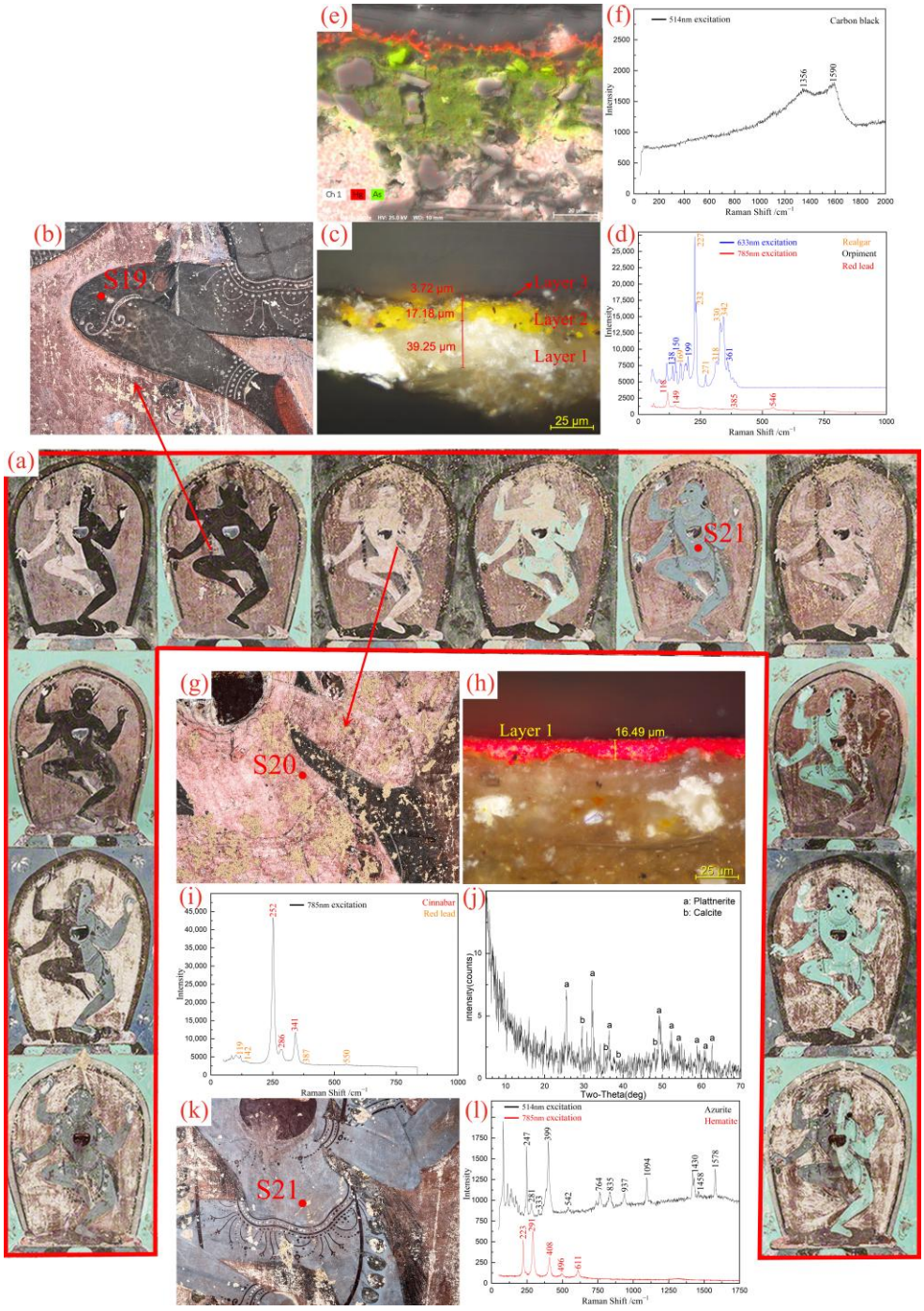


Figure 15. (**a**) Twelve animal-headed figures of the eastern panel on the northern wall; (**b**) right knee of the second black figure counting from the left in the upper zone; (**c**) photomicrograph of the pigment cross-section of S19 (500×); (**d**) Raman spectra of S19; (**e**) EDS elemental map showing Hg and As distribution for the cross-section of S19; (**f**) Raman spectrum of the black pigment grains of S19; (**g**) waist of the third pink figure counting from the left in the upper zone; (**h**) photomicrograph of

https://doi.org/10.3390/coatings16111348

the pigment cross-section of S20 (500×); (**i**) Raman spectrum of S20; (**j**) XRD pattern of S20; (**k**) abdomen of the fifth blue figure counting from the left in the upper zone; (**l**) Raman spectra of S21.

Sample S20 was taken from the waist of the third pink figure counting from the left in the upper zone. PLM of the cross-section shows a single, uniform red pigment layer approximately 16.5 μm thick with no internal stratification. Raman spectroscopy detects cinnabar and red lead, and XRD identifies plattnerite (Figure 15). It is therefore inferred that this region was painted with a mixture of red lead and cinnabar. As observed from the colour appearance of the mural, the colouring is thin and uneven, allowing the underlying white ground to show through. Hence, the overall colour is pale red.

Sample S21 was taken from the abdomen of the fifth blue figure counting from the left in the upper zone. Raman spectroscopy identifies azurite and hematite (Figure 15). In consideration of the visual appearance of the mural, it is tentatively interpreted that hematite was applied as the underlayer, with azurite overlaid on top.

According to the *Śrī-laghu-saṃvara*, the Saṃvara maṇḍala includes eight guardian goddesses. Four animal-faced ḍākinīs guard the four cardinal directions, with body colours of blue, yellow, red and green. The four attendants guard the four diagonal corners of the maṇḍala and are mostly depicted with bicoloured bodies. Their colour schemes are specified as follows: Yamadāhī (southeast), blue on the left and yellow on the right; Yamadūtī (southwest), yellow on the left and red on the right; Yamadaṃṣṭrī (northwest), red on the left and green on the right; Yamamathanī (northeast), green on the left and blue on the right [2,33]. Comparison reveals that the four monochromatic animal-headed figures also feature four colours in Cave 465. Blue and green are consistent with the textual record, while pink and deep orange show deviations. For the bicoloured-bodied figures in Cave 465, their colour schemes are: orange on the left and pink on the right; blue on the left and orange on the right; green on the left and blue on the right; red on the left and green on the right. The left-right colour arrangement and sequence are analogous to the textual prescriptions, with only orange and pink showing minor differences.

3.2.5. Deity Images on the Eastern Wall

Two panels are depicted on the eastern wall of the main chamber, on either side of the passageway doorway. The southern panel comprises three figures arranged in a triangular configuration. The uppermost figure is greyish-white, with partial pigment loss revealing an underlying reddish-brown layer. The two lower figures also have reddish-brown bodies overlaid with patchy white pigment. Close observation shows that the intrinsic body colour of the three figures is similar; they differ only in the thickness and preservation state of the superficial greyish-white pigment.

Sample S22 was taken from the chest of the upper figure. PLM of the cross-section reveals a single pigment layer composed of a mixture of blue and white pigments, with a thickness of approximately 14 μm. Raman spectroscopy identifies indigo, azurite and gypsum. The azurite peaks are weak, and Cu was not detected by XRF; it is therefore speculated that Cu originates from incidental impurities. Sample S23 was taken from the abdomen of the lower northern figure. Raman spectroscopy identifies plattnerite, and XRF analysis shows that Pb and Fe are the major characteristic elements (Figure 16). The Fe content is markedly higher than in other samples. Excluding the interference of Fe from the plaster ground, it is tentatively inferred that hematite may also be present in this sample. Given the similar colouration of the three figures, it is hypothesised that they were painted with a flat wash of red lead mixed with a small amount of hematite, followed by glazing or local washing with indigo mixed with gypsum on the overlayer.

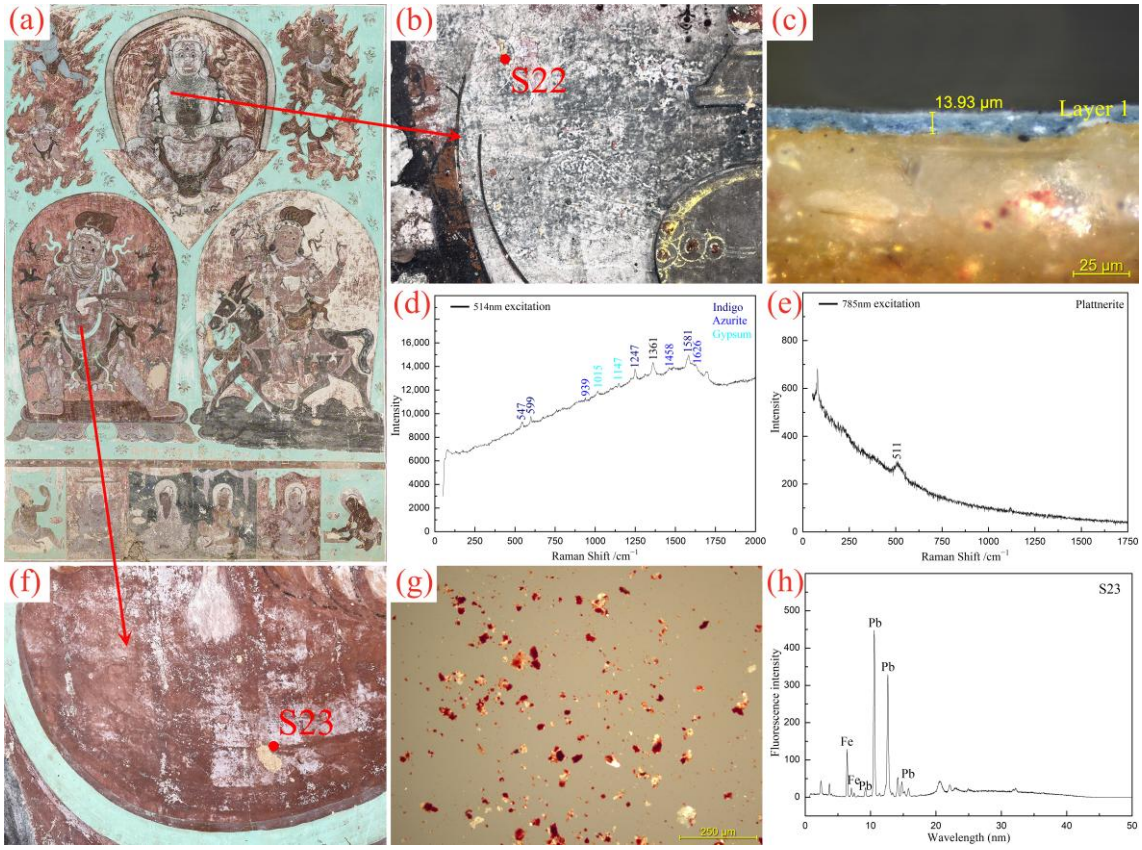


Figure 16. (**a**) Three figures of the southern panel on the eastern wall; (**b**) chest of the upper figure; (**c**) photomicrograph of the pigment cross-section of S22 (500×); (**d**) Raman spectrum of S22; (**e**) Raman spectrum of S23; (**f**) lower northern figure; (**g**) photomicrograph of pigment grains of S23 (200×, PPL); (**h**) XRF spectrum of S23.

Scholars identify these three figures as protective deities: the upper figure is Ekajaṭī, the lower northern figure is Mahākāla with a staff, and the southern figure riding a mule is Śrīdevī. According to the Tibetan iconographic text *Yi dam rgya mtsho'i sgrub thabs rin chen 'byung gnas kyi lhan thabs rin 'byung don gsal*, Ekajaṭī has a blue body and wears a white silk garment [19,34]. Mahākāla and Śrīdevī are typically depicted in bluish-black in thangkas. Comparison reveals that the original body colour of these three protective deities in Cave 465 is red, overlaid with grey-blue pigment of differing thicknesses. The upper figure bears a relatively thick overlayer of surface pigment, appearing grey-blue overall, which resembles the blue body with a white silk garment described in the textual prescriptions. The two lower figures are predominantly red with local grey-blue washes, so their dominant hue remains red, differing from the conventional colours used in thangkas.

A summary of the colouring techniques identified across these 23 sampling points reveals recurring patterns. First, cinnabar and red lead were used in combination. Samples S15, S18 and S20 employ both pigments, with distinct application modes: red lead was fully glazed over cinnabar in S15; cinnabar was locally washed over red lead in S18; and the two pigments were mixed together for application in S20. Second, azurite was used in combination with red pigments. This combination appears in S4, S7, S10, S13, S16, S17 and S21. Azurite was glazed over red lead in S7; azurite was overlaid on hematite in S4, S17 and S21; and azurite was mixed with minor hematite in S10, S13 and S16. Third, indigo was combined with red lead. S6, S12 and S14 were painted with indigo following the same procedure: red lead was washed over indigo. By contrast, S22 and S23 adopt the reverse sequence: red lead forms the underlayer, and indigo mixed with a small amount of white pigment is applied as the overlayer. Fourth, orpiment was used in combination with red pigments. S2 and S9 feature an orpiment

underlayer glazed with red lead, whereas S19 has an orpiment underlayer glazed with cinnabar. In addition, red lead was used alone, as seen in S8 and S11 (Table 3).

Table 3. Analytical results of the colouring techniques used in the murals of Cave 465.

Material Combination	Sample No.	Colouring Technique	Present Colour	Inferred Original Colour	Textual Prescription
Cinnabar and red lead	S15	Cinnabar + red lead (glazed)	Pink	Warm pink	Red
	S18	Red lead + cinnabar (local washing)	Reddish-brown	Red	/
	S20	Cinnabar + red lead (mixed)	Pale red	Pale red	Red
Azurite with red lead and hematite	S7	Red lead + azurite (glazed)	Purplish-brown	Purplish-red	Dark blue
	S4	Hematite + azurite (thick application)	Vivid blue	Vivid blue	Blue
	S17, S21	Hematite + azurite (thin application)	Dark greyish-blue	Dark greyish-blue	Dark blue/blue
	S10, S16	Azurite mixed with trace hematite	Vivid blue	Vivid blue	Blue
	S13	Azurite mixed with minor hematite	Greyish-blue	Greyish-blue	Blue
Indigo and red lead	S6, S12, S14	Indigo + red lead (glazed)	Bluish-black	Dark blue	Dark blue/blue
	S22, S23	Red lead + indigo/white pigment (glazed)	Reddish-brown + greyish-white	Red + greyish-blue	Blue+white
Orpiment with red lead and cinnabar	S2	Orpiment + red lead (thin application)	Blackish-brown	Pale orange-yellow	Golden yellow
	S9	Orpiment + red lead (thick application)	Reddish-brown	Warm red	Red
	S19	Orpiment + cinnabar/carbon black (glazed)	Black	Deep orange-yellow	Yellow
Red lead	S8, S11	Red lead	Reddish-brown	Red	Red
Atacamite	S5	Atacamite	Green	Green	Green
Indigo and white pigment	S1	Gypsum/calcite + indigo/carbon black (glazed)	Greyish-black	Bluish-black	White
Cinnabar and lac dye	S3	Cinnabar + lac dye (mixed)	Pale red	Pale red	Red

4. Conclusions

Scientific analyses of pigments and colouring techniques based on 23 detection points from the murals of Mogao Cave 465 led to the following conclusions:

(1) The pigments used for painting the murals include mineral pigments such as red lead, cinnabar, hematite, atacamite, azurite, orpiment, gypsum, calcite, quartz, muscovite, kaolinite and albite, the inorganic pigment carbon black, as well as the organic pigments indigo and lac dye. These pigments were applied either individually, or by superimposition and mixing, to produce a wide range of colour effects.

(2) Unlike murals in other Mogao caves, azurite (the blue pigment) in Cave 465 was not used alone. Instead, it was employed together with red lead or hematite via superimposition or mixing. For superimposed application, the blue appears more vivid on the mural when the upper azurite layer is thicker than the underlying red pigment layer; the blue takes on a greyish tone when the upper azurite layer is thinner than the underlying red layer. The same trend applies to mixed application: the blue becomes greyer as the proportion of admixed red pigment increases.

(3) Based on the analytical results obtained in this study, colour alteration has only been observed in red lead. Discolouration occurs in areas where red lead was used alone, or in combination with azurite or indigo; the original red hue has transformed into the present reddish-brown. Nevertheless, regions where red lead was applied together with cinnabar do not exhibit substantial darkening. Where red lead was glazed over an underlying cinnabar layer, it is inferred that limited discolouration of the overlying red lead causes the overall colour to shift from warm pink to cool pink or purplish pink. For mural areas where the two pigments were mixed, no obvious darkening is visible

to the naked eye, and the tone remains relatively red. This observation is broadly consistent with the findings on red lead discolouration in Reference [35].

(4) Field investigation reveals that no yellow hues are visible in the present colour of the murals in Cave 465. However, instrumental analysis demonstrates that orpiment was employed as the underlayer in many regions. Alongside the samples S2, S9 and S19 examined in this study, previous investigations reported in Reference [24] also indicate that orpiment, a yellow pigment, was widely used in Cave 465. It was not applied independently; instead, colour expression was achieved by glazing with red lead or cinnabar over the orpiment underlayer. It may be inferred that this technique was intended to achieve a more restrained yellow hue—orange-yellow or warm yellow—to replace the bright yellow of orpiment.

(5) By analysing the painting materials and techniques of the iconographic figures in Cave 465, and comparing them with the corresponding iconographic prescriptions for the deities identified by previous scholars as well as conventional colours used in thangkas, it is found that the body colour and spatial arrangement of the Five Buddhas on the ceiling, the colour schemes of most Vajra deities and their consorts, and the left-right colour arrangement of the two-coloured directional guardian goddesses in Cave 465 show similarities to textual records. Only a few individual colours differ in expression. For instance, blue pigments in Cave 465 were applied in more diverse and complex ways, yielding not a uniform blue but blues of varied tones.

Author Contributions: Writing—original draft, D.L.; formal analysis, D.L., J.Z.; investigation, D.L., J.Z.; validation, Y.Y.; writing–review and editing, Y.Y.; supervision, Z.Y. All authors have read and agreed to the published version of the manuscript.

Funding: This study was supported by the National Cultural Heritage Administration of the People's Republic of China (NCHA) (National Archaeological Talent Revitalization Program, Grant No. (2025-204), the Gansu Provincial Department of Science and Technology (Gansu Science and Technology Program-Youth Fund, Grant No. 23JRRF0009), the Gansu Provincial Department of Science and Technology (Basic Research Innovation Group Program, Grant No. 24JRRF001), and Dunhuang Municipal Bureau of Science and Technology (Dunhuang Municipal Science and Technology Program) for the projects "Research on Scientific Approaches to Understanding the Materials and Techniques of Dunhuang Mural Plaster" and "Research on the Evolutionary Patterns of Chronological Characteristics of Materials and Techniques of Mogao Grottoes Murals".

Institutional Review Board Statement: Not applicable.

Informed Consent Statement: Not applicable.

Data Availability Statement: The datasets used and analyzed during the current study are available from Dandan Li (ldd20397@dha.ac.cn) on reasonable request.

Conflicts of Interest: The authors declare no conflicts of interest.

Appendix A

Figure A1 shows the total ion chromatogram (TIC) obtained from the THM-Py-GC/MS analysis of the gray pigment sample collected from the Buddha figure in the center of the ceiling panel. Table A1 presents detailed information on the pyrolysis products.

As shown in Table A1, Peaks 1–52 correspond to pyrolysis products derived from proteinaceous binding media in the sample. With fingerprint peaks of animal glue (1H-Pyrrole, 3-methyl-) detected [36,37], and considering the relative proportions of the identified compounds, including Blood-unverified 6 (5.9%), Protein 1—tofu and blood (30.0%), Protein 3—blood & glue (18.9%), 1H-Pyrrole, 1-methyl- (8.0%), Hydroxyproline methylated (4.0%), d-Proline, N-methoxycarbonyl-, methyl ester (3.7%), Glue-unverified 3

(25.2%), and Protein 131–160 (casein, egg white) (2.2%) [27],it is further inferred that the proteinaceous binding medium is consistent with animal glue.

Peaks 53–79 correspond to characteristic pyrolysis products of indigo. Among these compounds, anthranilic acid, methyl ester and N-Methyl anthranilic acid, methyl ester are characteristic pyrolysis products serving as molecular markers for indigo.

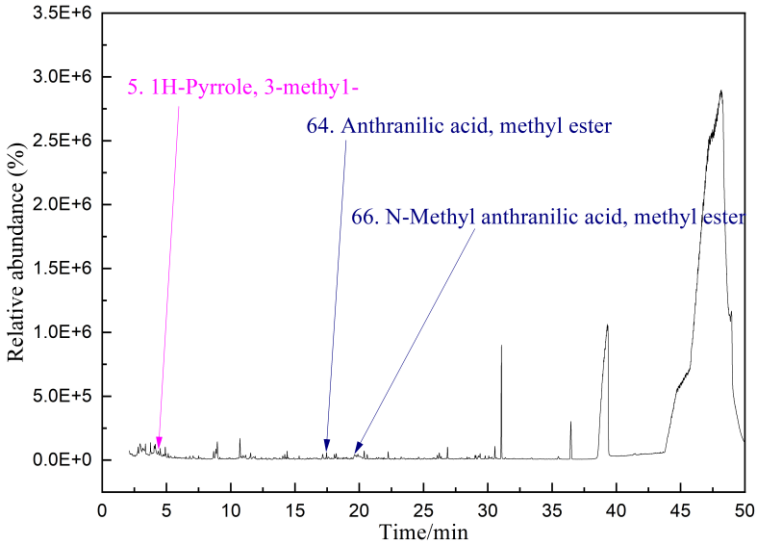


Figure A1. TIC chromatogram obtained from the THM-Py-GC/MS analysis of the sample.

Table A1. Results of THM-Py-GC/MS Analysis on Sample.

No.	RT/min	RI	Name	No.	RT/min	RI	Name
			Animal Glue				
1	2.2754	682.2	Benzene	27	12.6814	1157.9	Benzene, 1,4-dimethoxy-
2	2.9197	746.3	Pyrrole	28	12.7275	1159.4	Naphthalene, 1,2-dihydro-
3	3.1064	760.1	Toluene	29	13.3367	1179.8	Naphthalene
4	3.3605	780.8	Propanoic acid, 2-methoxy-, methyl ester	30	14.0366	1207.9	Blood—unverified 10
5	4.2216	832.5	1H-Pyrrole, 3-methyl-	31	14.1999	1213.7	Protein—unverified 8
6	5.1361	879.8	N,N-Dimethyl-L-alanine methyl ester	32	14.298	1217.3	Protein 56-141-156 (glue, egg white, yolk, casein)
7	5.336	890.2	Styrene	33	14.4584	1223	Hydroxyproline methylated
8	5.3806	892.5	o-Xylene	34	15.5823	1263.5	Blood—unverified 11
9	5.5776	901.1	Pentanoic acid, 3-methyl-2-oxo-, methyl ester	35	16.2801	1288.6	1-Tridecene
10	5.8016	911.1	2,3-Dimethoxypropan-1-ol	36	16.8051	1307.8	Naphthalene, 1-methyl-
11	5.9071	915.8	Anisole	37	17.4509	1332.2	L-Proline, 1-methyl-5-oxo-, methyl ester
12	6.1011	924.6	Dimethyl sulfone	38	18.6414	1377.1	Biphenyl
13	6.2073	928.5	2(5H)-Furanone	39	18.681	1378.6	d-Proline, N-methoxycar-bonyl-, methyl ester
14	7.0735	959.9	Benzaldehyde	40	19.7544	1420.1	Blood—unverified 6
15	7.6299	981.2	Phenol	41	20.3804	1445	1,2-Dimethyl phthalate
16	7.8196	988.5	1-Decene	42	20.6162	1454.3	Glue—unverified 2
17	8.6338	1023.3	2-Methylanisole	43	22.5741	1533.9	Glue marker (fish glue 126/158-2)
18	8.6697	1024.9	Dimethyl fumarate	44	23.2594	1562.6	Blood—unverified 1
19	8.8417	1031.6	1-Hexanol, 2-ethyl-	45	26.0864	1685.3	Protein 3—blood & glue

20	9.1983	1043.2	L-Proline, 1-methyl-, methyl ester	46	26.227	1691.5	Protein 1—tofu and blood
21	9.2979	1046.4	Indene	47	26.6107	1709.2	Protein 131-160 (casein, egg white)
22	9.3447	1047.9	2-Pyrrolidinone, 1-methyl-	48	26.9453	1725.3	Protein 131-175 (glue, egg white, yolk, casein)
23	9.9005	1065.9	Benzenamine, 3 methyl	49	26.9563	1725.8	N-(p-Vinylbenzoyl)-l-alanine
24	9.9393	1067.2	Acetophenone	50	29.3981	1843.3	Glue—unverified 3
25	11.4535	1116.8	Methyl 1-methylpyrrole-2-carboxylate	51	33.4164	2024.6	1-Octadecanol, methyl ether
26	12.4178	1149	p-Methoxystyrene	52	46.3097	2699.2	Heptacosane
			Indigo				
53	4.6858	856.5	Benzene, 1,3-dimethyl- (and 1,4 isomer)	67	20.3043	1441.9	Octanedioic acid, dimethyl ester
54	6.0638	922.9	Hexanoic acid, methyl ester	68	21.6186	1494.1	1,4-Benzenedicarboxylic acid, dimethyl ester
55	8.6989	1026.2	Heptanoic acid, methyl ester	69	22.2512	1520.4	Dodecanoic acid, methyl ester
56	8.8088	1030.6	Benzene, cyclopropyl-	70	22.7732	1542.2	Nonanedioic acid, dimethyl ester
57	8.9545	1035.3	Butanedioic acid, dimethyl ester	71	26.8633	1721.4	Tetradecanoic acid, methyl ester
58	9.147	1041.5	Hexanoic acid, 2-ethyl-, methyl ester	72	28.5612	1803	1,2,3-Benzenetricarboxylic acid, trimethyl ester
59	11.5538	1120.1	Octanoic acid, methyl ester	73	29.0064	1824.4	Pentadecanoic acid, methyl ester
60	11.9045	1131.9	Pentanedioic acid, dimethyl ester	74	29.0701	1827.5	1,2,4-Benzenetricarboxylic acid, trimethyl ester
61	14.394	1220.7	Nonanoic acid, methyl ester	75	30.5484	1898.6	Palmitoleic acid, methyl ester
62	14.919	1239.6	Hexanedioic acid, dimethyl ester	76	31.0588	1923.1	Hexadecanoic acid, methyl ester
63	17.1477	1320.7	Decanoic acid, methyl ester	77	33.3637	2022.8	Heptadecanoic acid, methyl ester
64	17.6178	1338.5	Anthranilic acid, methyl ester	78	35.4973	2093.1	9-Octadecenoic acid (Z)-, methyl ester
65	18.4899	1371.4	Benzoic acid, 4-methoxy-, methyl ester	79	36.4609	2124.8	Octadecanoic acid, methyl ester
66	19.3392	1403.6	N-Methyl anthranilic acid, methyl ester				

Figure A2 shows the total ion chromatogram (TIC) obtained from the THM-Py-GC/MS analysis of the red pigment sample collected from the Buddha figure on the western sloping ceiling panel. Table A2 provides detailed information on the pyrolysis products.

As shown in Table A2, Peaks 1–63 correspond to pyrolysis products derived from proteinaceous binding media in the sample. With fingerprint peaks of animal glue (1H-Pyrrole, 1-methyl-, 1H-Pyrrole, 3-methyl-, Diketo-dipyrrole) detected [36,37], and considering the relative proportions of the identified compounds, including Blood-unverified 5 (4.9%), Blood-unverified 6 (5.7%), Protein 1—tofu and blood (21.4%), Blood-unverified 7 (0.8%), Protein 3—blood & glue (7.3%), 1H-Pyrrole, 1-methyl- (30.3%), Hydroxyproline methylated (5.2%), d-Proline, N-methoxycarbonyl-, methyl ester (5.3%), Glue-unverified 3 (11.5%), and Protein 131–160 (casein, egg white) (6.1%) [27], it is further inferred that the proteinaceous binding medium is consistent with animal glue.

https://doi.org/10.3390/coatings16111348

Peaks 64–97 correspond to characteristic pyrolysis products associated with indigo and shellac resin. Among these compounds, Anthranilic acid, methyl ester and N-methyl anthranilic acid, methyl ester are characteristic pyrolysis products of indigo, whereas Butolic acid, 6-methoxy, methyl ester, 8-Methoxyhexadecanoic acid, methyl ester, 9,10-Dimethoxyhexadecanoic acid, methyl ester are characteristic pyrolysis products associated with shellac resin.

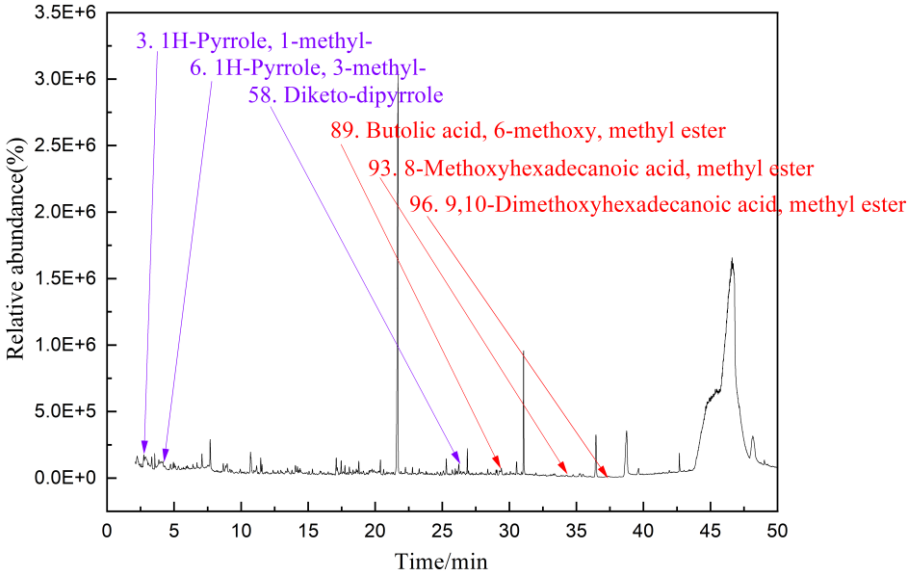


Figure A2. TIC chromatogram obtained from the THM-Py-GC/MS analysis of the sample.

Table A2. Results of THM-Py-GC/MS Analysis on Sample.

No.	RT/min	RI	Name	No.	RT/min	RI	Name
Animal Glue							
1	2.2717	681.6	Benzene	33	13.3374	1179.8	Naphthalene
2	2.6371	725.4	Propanoic acid	34	13.7731	1198.1	Benzene, (1,2-dimethoxyethyl)-
3	2.744	733.3	1H-Pyrrole, 1-methyl-	35	13.7855	1198.6	m-Isopropylphenol
4	3.0793	758.1	Toluene	36	14.0286	1207.6	Blood—unverified 10
5	3.3363	778.8	Propanoic acid, 2-methoxy-, methyl ester	37	14.1985	1213.7	Protein—unverified 8
6	4.2062	831.7	1H-Pyrrole, 3-methyl-	38	14.2922	1217.1	Protein 56-141-156 (glue, egg white, yolk, casein)
7	4.6762	856	Benzene, 1,3-dimethyl- (and 1,4 isomer)	39	14.4459	1222.6	Hydroxyproline methylated
8	4.6762	856	Ethyl benzene	40	15.5918	1263.8	Blood—unverified 11
9	4.8871	866.9	o-Xylene	41	15.884	1274.3	1,2-Benzenediol, 3-methyl-
10	5.0057	873.1	2-Propanol, 1,3-dimethoxy-	42	16.2911	1289	1-Tridecene
11	5.1119	878.6	N,N-Dimethyl-L-alanine methyl ester	43	16.417	1293.5	Naphthalene, 1-methyl-
12	5.3345	890.1	Styrene	44	17.2232	1323.6	Blood—unverified 5
13	5.5768	901	Pentanoic acid, 3-methyl-2-oxo-, methyl ester	45	17.4589	1332.5	L-Proline, 1-methyl-5-oxo-, methyl ester
14	5.6332	903.6	2-Cyclopenten-1-one, 2-methyl-	46	18.6854	1378.8	d-Proline, N-methoxycarbonyl-, methyl ester
15	5.6947	906.3	2,3-Dimethoxypropan-1-ol	47	18.9585	1389.1	1-Tetradecene
16	7.0749	960	Benzaldehyde	48	19.7199	1418.7	N-Methylphthalimide
17	7.6394	981.6	Phenol	49	19.7632	1420.5	Blood—unverified 6

18	7.8064	988	1-Decene	50	20.3855	1445.2	1,2-Dimethyl phthalate
19	8.6316	1023.2	2-Methylanisole	51	20.625	1454.7	Glue—unverified 2
20	8.6682	1024.9	Dimethyl fumarate	52	22.5785	1534.1	Glue marker (fish glue 126/158-2)
21	8.8051	1030.5	Benzene, cyclopropyl-	53	23.277	1563.4	Blood—unverified 1
22	8.8483	1031.9	1-Hexanol, 2-ethyl-	54	23.7983	1585.2	3,4-dimethoxy benzoic acid, methyl ester
23	9.1712	1042.3	L-Proline, 1-methyl-, methyl ester	55	25.7423	1670.2	Methyl p-methoxycinnamate, cis
24	9.3118	1046.9	2-Pyrrolidinone, 1-methyl-	56	26.0871	1685.4	Protein 3—blood & glue
25	9.5453	1054.4	Phenol, 2-methyl-	57	26.2351	1691.9	Protein 1—tofu and blood
26	9.9356	1067.1	Acetophenone	58	26.3383	1696.4	Diketo-dipyrrole
27	10.7081	1092.1	2,5-Pyrrolidinedione, 1-methyl-	59	26.6121	1709.3	Protein 131-160 (casein, egg white)
28	11.4593	1117	Methyl 1-methylpyrrole-2-carboxylate	60	26.9585	1725.9	Protein 131-175 (glue, egg white, yolk, casein)
29	12.141	1139.8	1,2-Dimethoxybenzene	61	27.7829	1765.6	Drying oil—unverified 1
30	12.4207	1149.1	p-Methoxystyrene	62	28.4639	1798.3	Blood—unverified 7
31	12.696	1158.4	Benzene, 1,4-dimethoxy-	63	29.4033	1843.5	Glue—unverified 3
32	12.7443	1160	Naphthalene, 1,2-dihydro-				
			Indigo and shellac resin				
64	6.0594	922.7	Hexanoic acid, methyl ester	81	20.3021	1441.9	Octanedioic acid, dimethyl ester
65	8.6982	1026.2	Heptanoic acid, methyl ester	82	21.9253	1506.7	1,3-Benzenedicarboxylic acid, dimethyl ester
66	8.9589	1035.4	Butanedioic acid, dimethyl ester	83	26.4679	1702.4	Dimethyl methoxybenzene dicarboxylate isomer 2
67	9.1478	1041.6	Hexanoic acid, 2-ethyl-, methyl ester	84	26.637	1710.5	Benzoic acid, 3,4,5-trimethoxy-, methyl ester
68	10.7425	1093.2	Benzoic acid, methyl ester	85	26.8647	1721.4	Tetradecanoic acid, methyl ester
69	11.0149	1102.1	Benzene, 1-isocyano-3-methyl-	86	28.5642	1803.2	1,2,3-Benzenetricarboxylic acid, trimethyl ester
70	11.5545	1120.1	Octanoic acid, methyl ester	87	29.0064	1824.4	Pentadecanoic acid, methyl ester
71	11.9125	1132.1	Pentanedioic acid, dimethyl ester	88	29.1023	1829	1,2,4-Benzenetricarboxylic acid, trimethyl ester
72	14.1194	1210.8	Benzoic acid, 3-methyl-, methyl ester	89	29.6676	1856.2	Butolic acid, 6-methoxy, methyl ester
73	14.3954	1220.8	Nonanoic acid, methyl ester	90	30.5477	1898.5	Palmitoleic acid, methyl ester
74	14.9167	1239.5	Hexanedioic acid, dimethyl ester	91	31.058	1923.1	Hexadecanoic acid, methyl ester
75	17.147	1320.7	Decanoic acid, methyl ester	92	33.3571	2022.6	Heptadecanoic acid, methyl ester
76	17.5366	1335.4	Benzoic acid, 3-methoxy-, methyl ester	93	34.2153	2050.9	8-Methoxyhexadecanoic acid, methyl ester
77	17.6281	1338.9	Anthranilic acid, methyl ester	94	35.4937	2093	9-Octadecenoic acid (Z)-, methyl ester
78	17.6625	1340.2	Heptanedioic acid, dimethyl ester	95	36.4558	2124.7	Octadecanoic acid, methyl ester
79	18.4957	1371.6	Benzoic acid, 4-methoxy-, methyl ester	96	37.4472	2172.2	9,10-Dimethoxyhexadecanoic acid, methyl ester

80	19.3399	1403.7	N-Methyl anthranilic acid, methyl ester	97	49.0137	2980	1-Octacosanol, methyl ether (Sutherland)

Appendix B

Figures A3–A9 below show the SEM-EDS spot analysis and mapping results for sample S02.

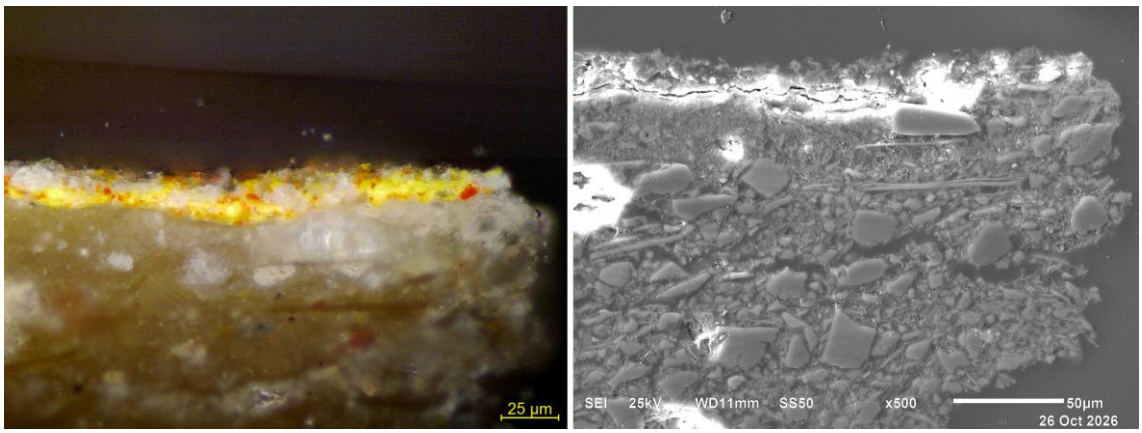


Figure A3. PLM photomicrograph (500×) and SEM micrograph (500×) of the cross-section of sample S02.

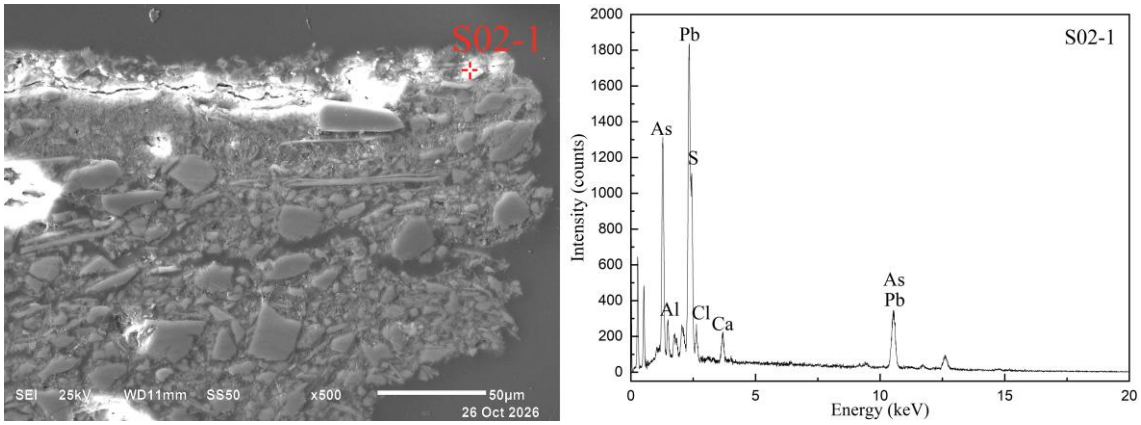


Figure A4. SEM micrograph of sample S02 cross-section and EDS spot spectrum of point S02-1.

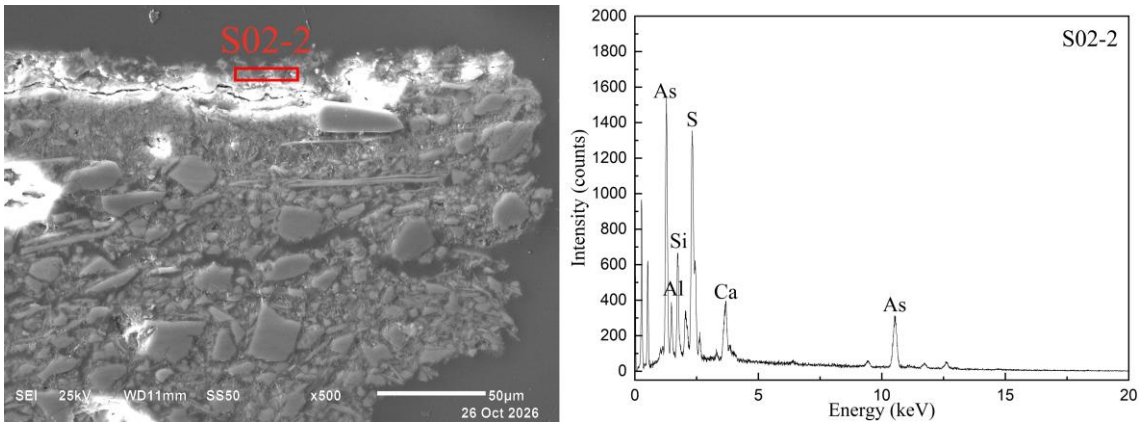


Figure A5. SEM micrograph of sample S02 cross-section and EDS area spectrum of region S02-2.

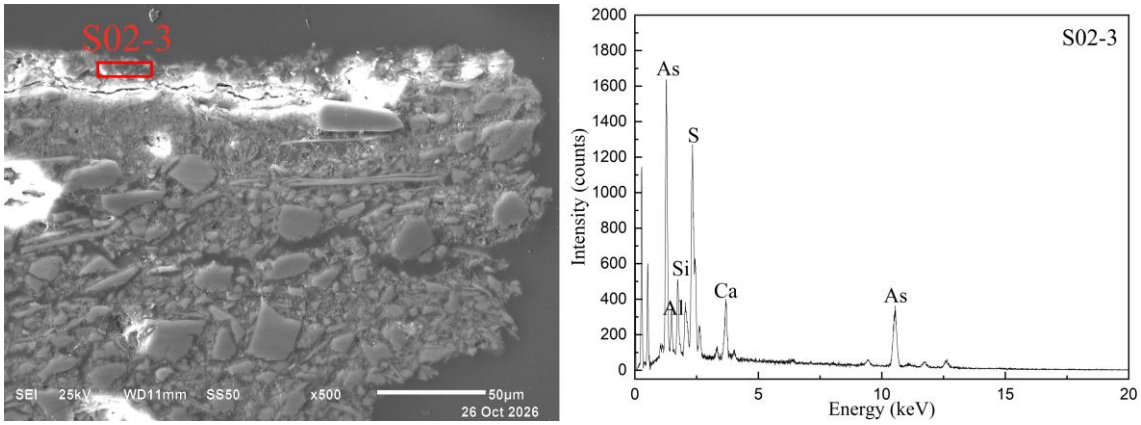


Figure A6. SEM micrograph of sample S02 cross-section and EDS area spectrum of region S02-3.

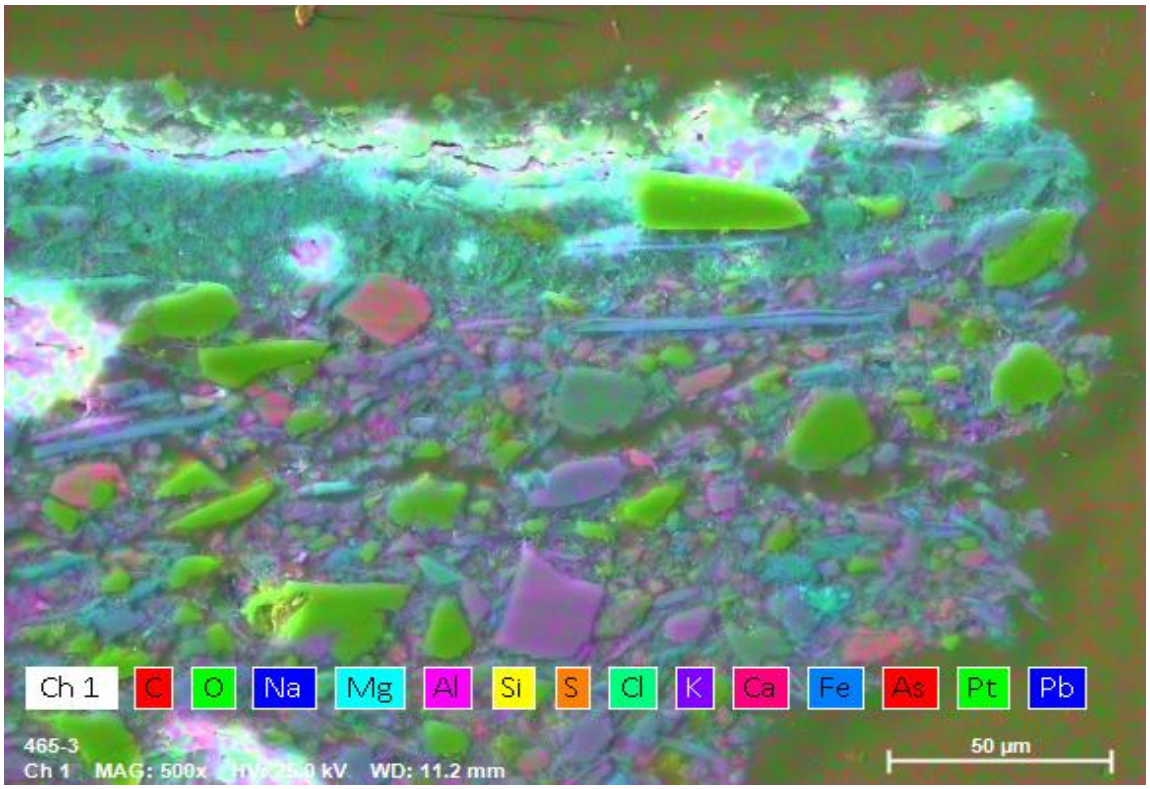


Figure A7. EDS elemental overlay map of sample S02 cross-section.

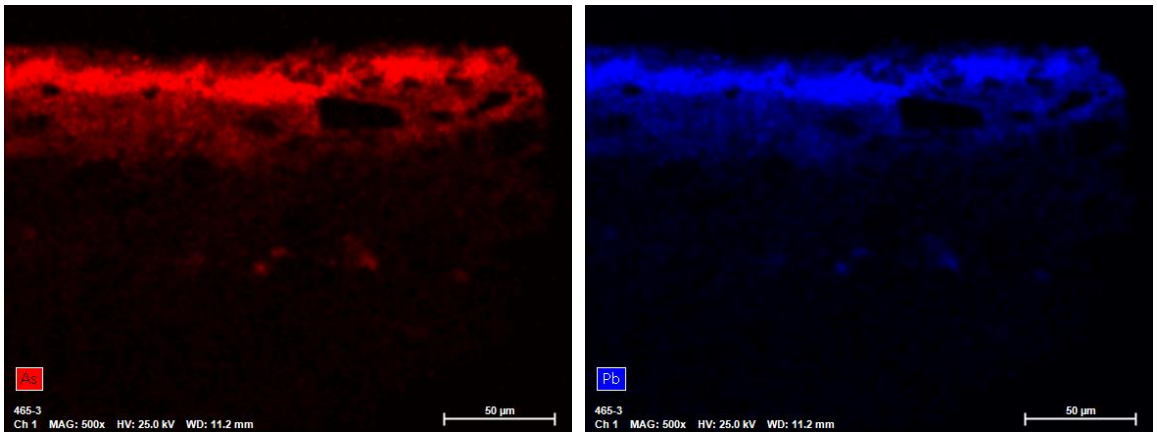


Figure A8. As and Pb EDS elemental maps of sample S02 cross-section.

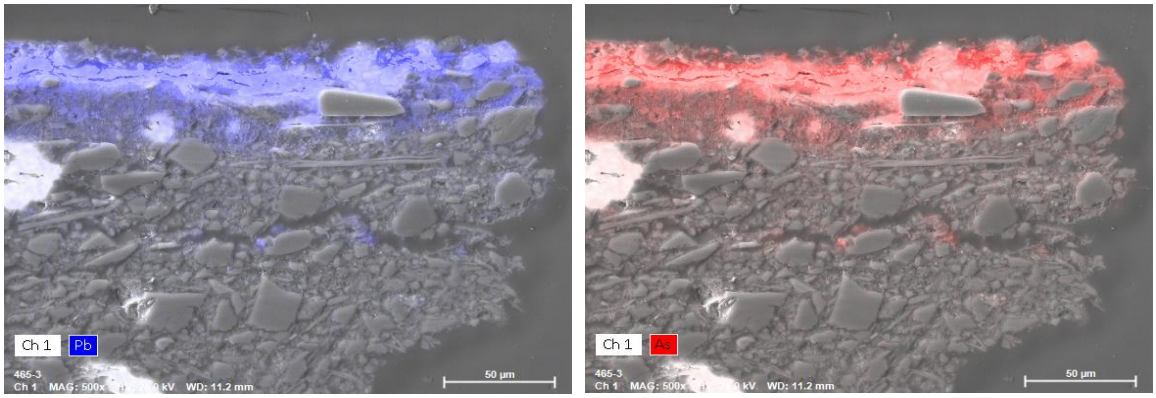


Figure A9. As and Pb EDS elemental maps overlaid on the SEM micrograph of sample S02 cross-section.

Appendix C

Figures A10–A15 below show the SEM-EDS spot analysis and mapping results for sample S12.

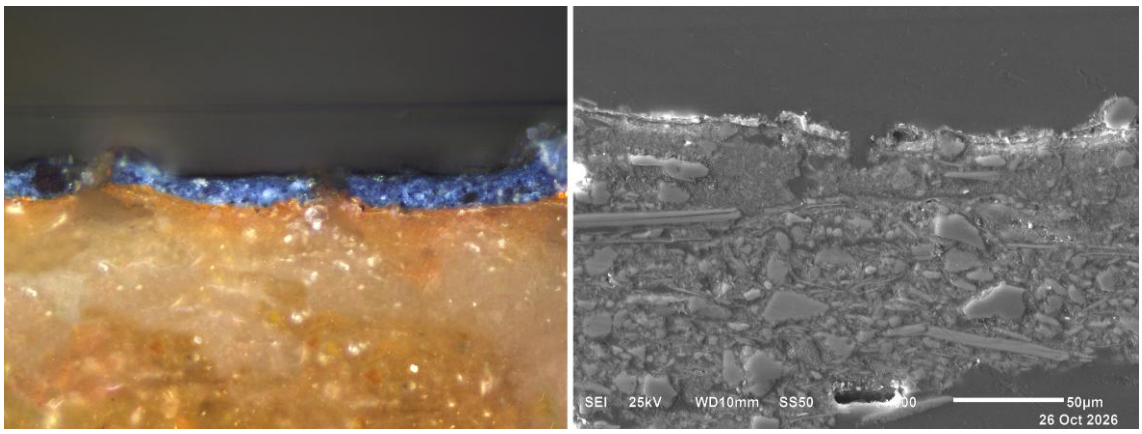


Figure A10. PLM photomicrograph (500×) and SEM micrograph (500×) of the cross-section of sample S12.

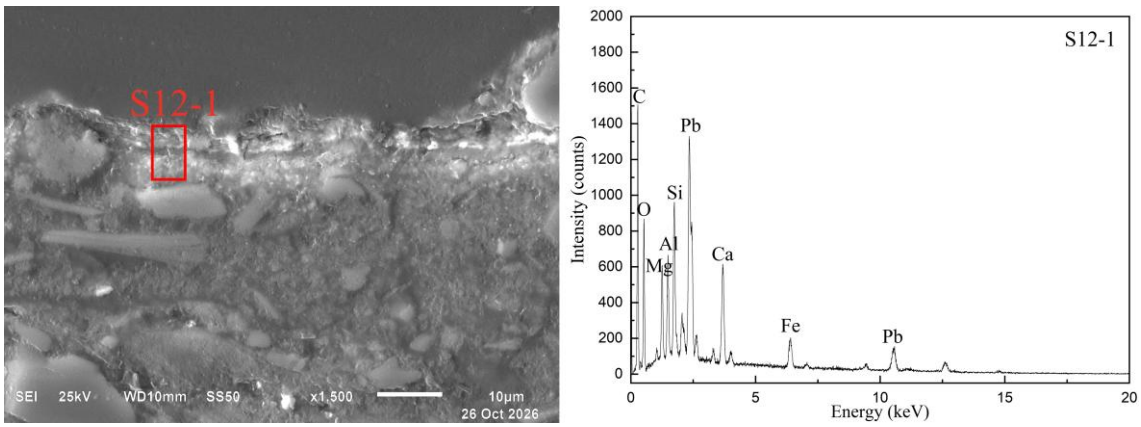


Figure A11. SEM micrograph of sample S12 cross-section and EDS area spectrum of region S12-1.

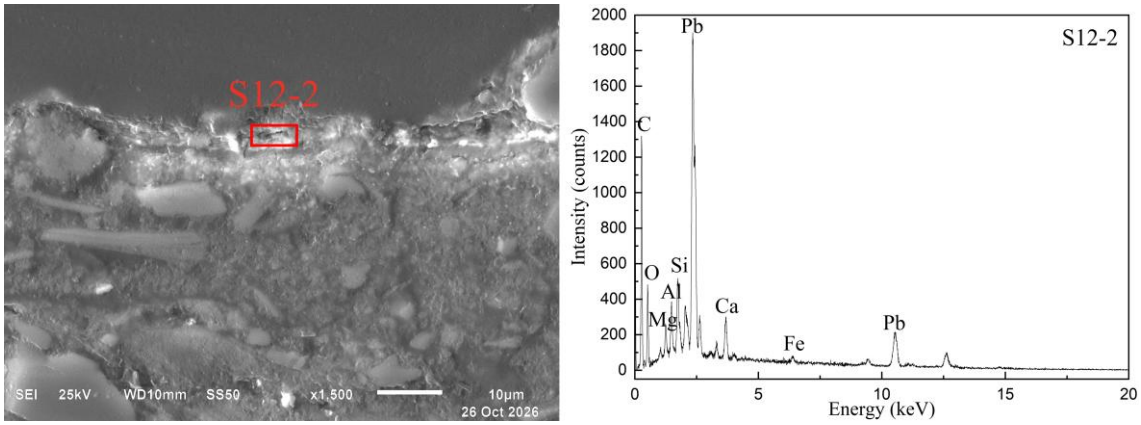


Figure A12. SEM micrograph of sample S12 cross-section and EDS area spectrum of region S12-2.

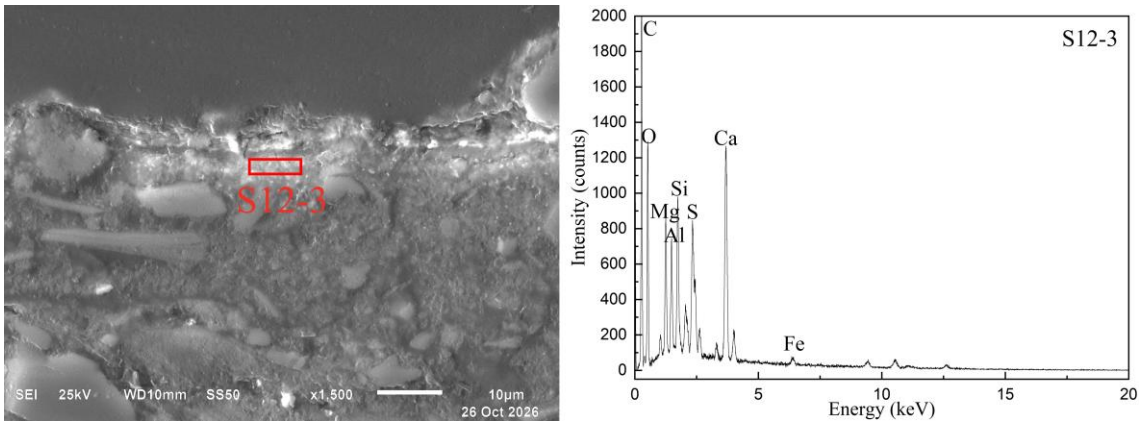


Figure A13. SEM micrograph of sample S12 cross-section and EDS area spectrum of region S12-3.

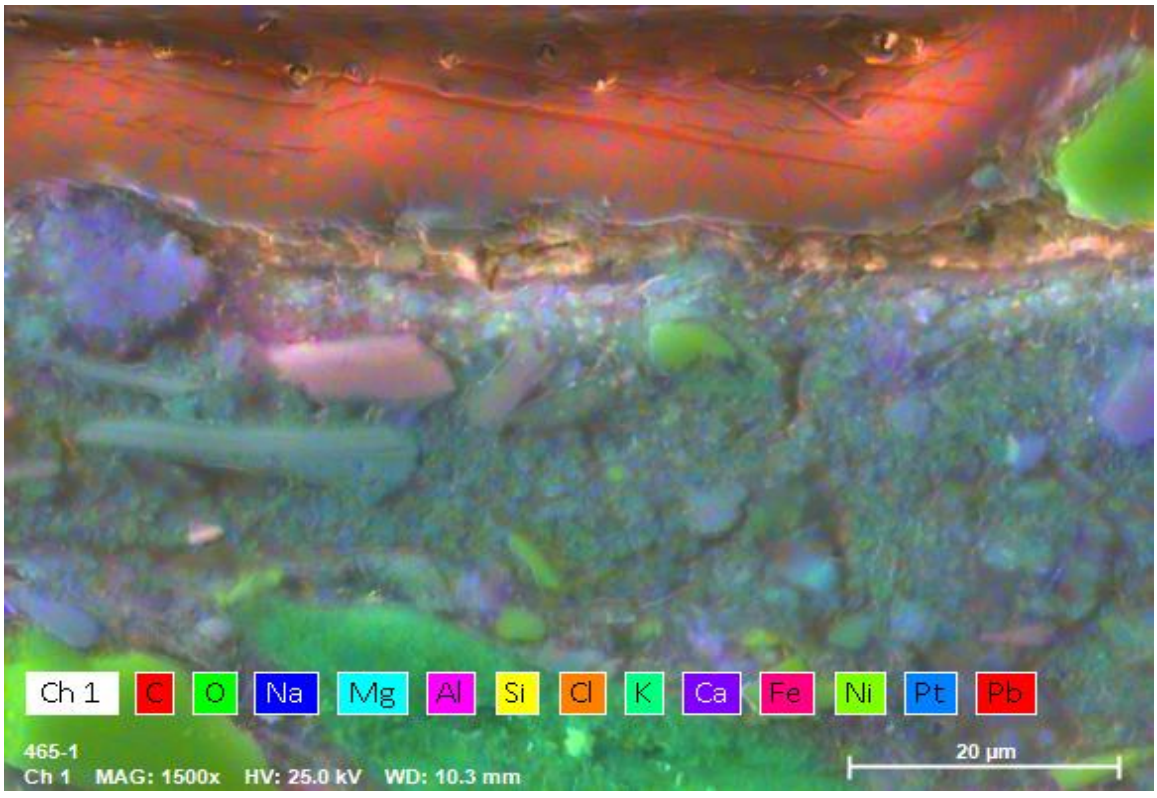


Figure A14. EDS elemental overlay map of sample S12 cross-section.

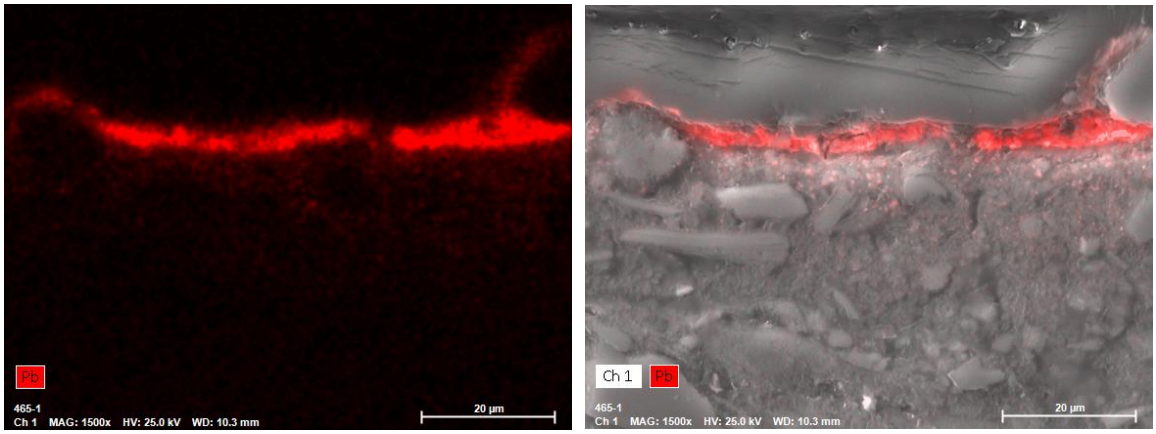


Figure A15. Pb EDS elemental map (**left**) and Pb elemental map overlaid on SEM micrograph (**right**), sample S12 cross-section.

Appendix D

Figures A16–A23 below show the SEM-EDS spot analysis and mapping results for sample S15.

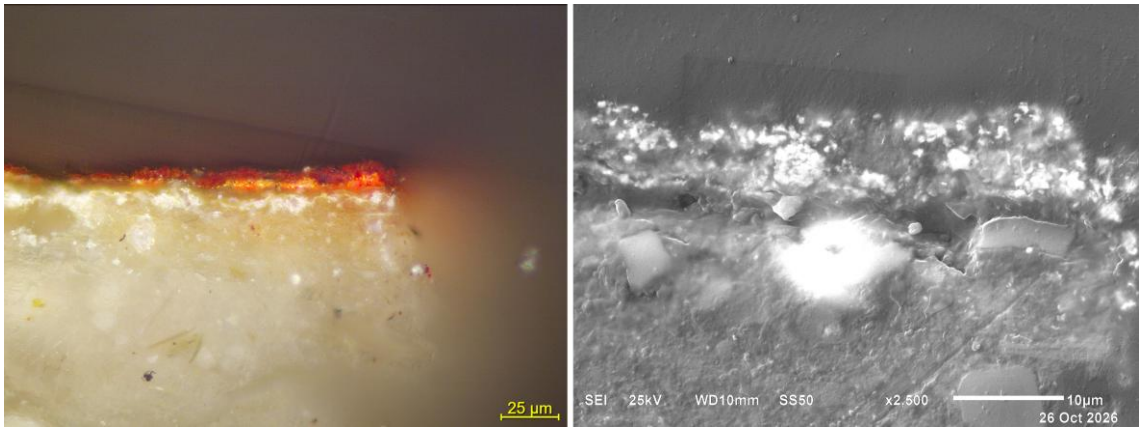


Figure A16. PLM photomicrograph (500×) and SEM micrograph (2500×) of the cross-section of sample S15.

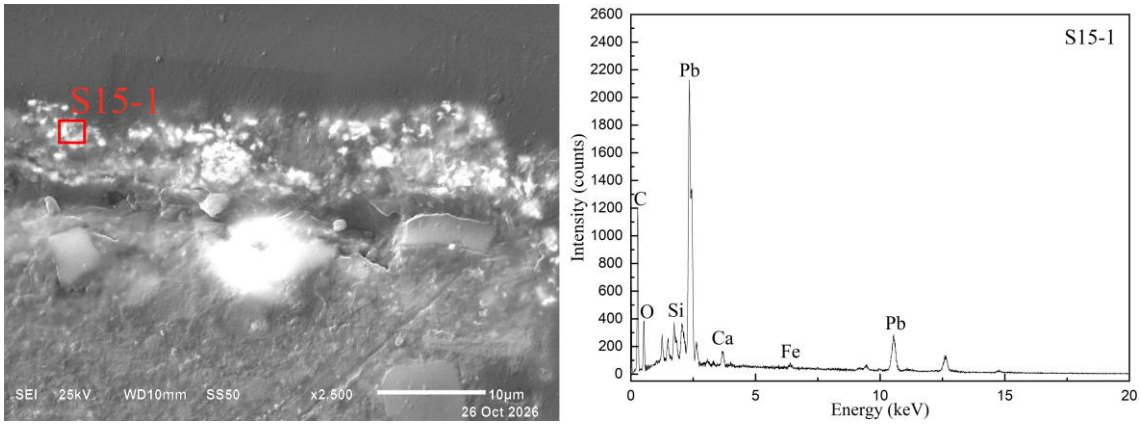


Figure A17. SEM micrograph of sample S15 cross-section and EDS area spectrum of region S15-1.

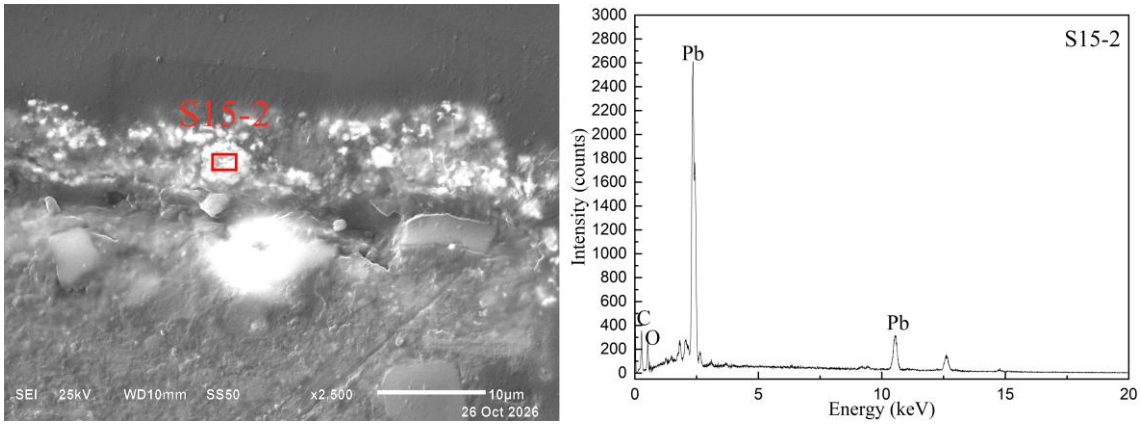


Figure A18. SEM micrograph of sample S15 cross-section and EDS area spectrum of region S15-2.

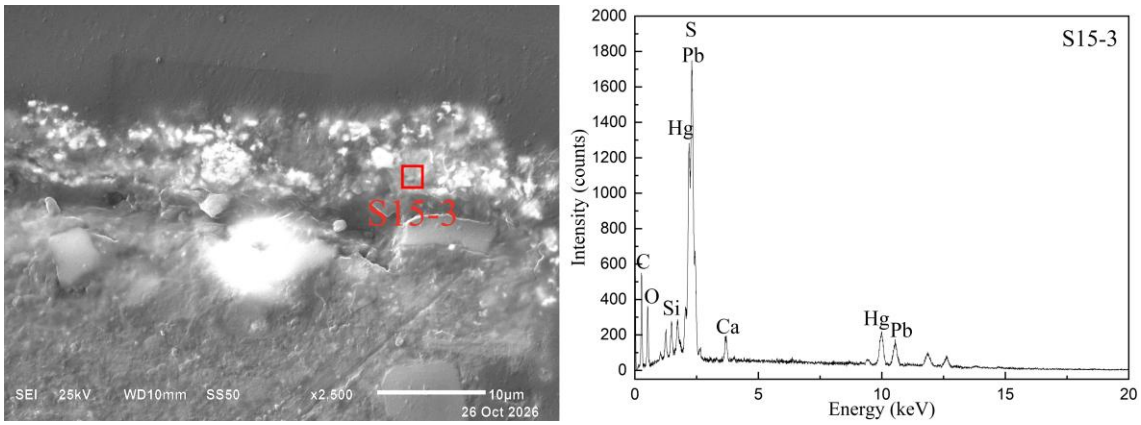


Figure A19. SEM micrograph of sample S15 cross-section and EDS area spectrum of region S15-3.

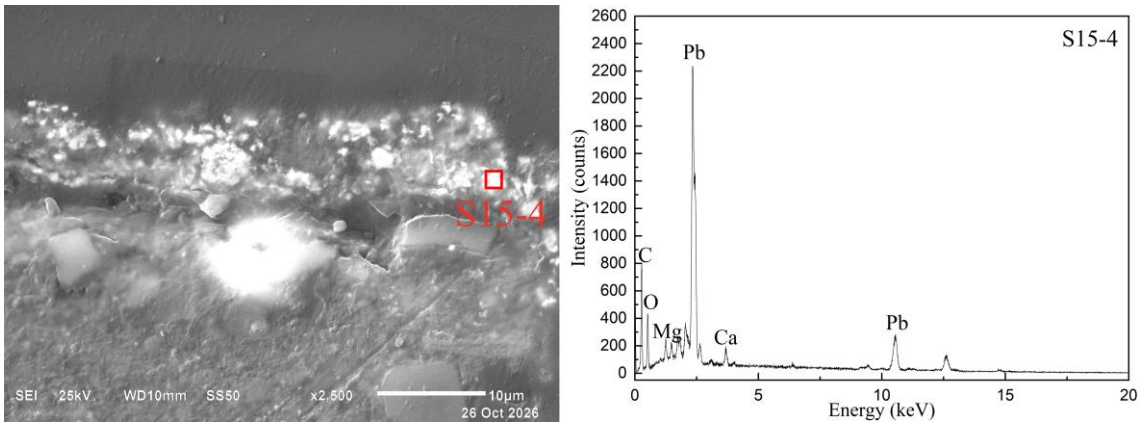


Figure A20. SEM micrograph of sample S15 cross-section and EDS area spectrum of region S15-4.

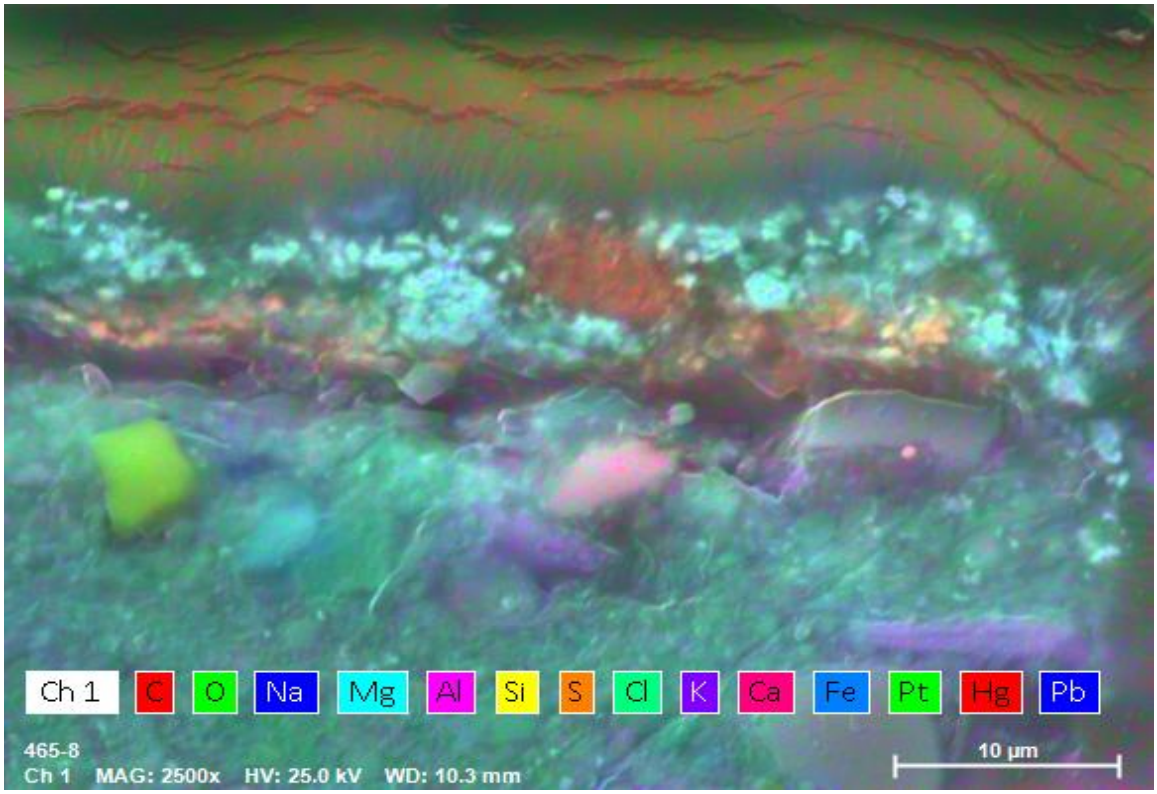


Figure A21. EDS elemental overlay map of sample S15 cross-section.

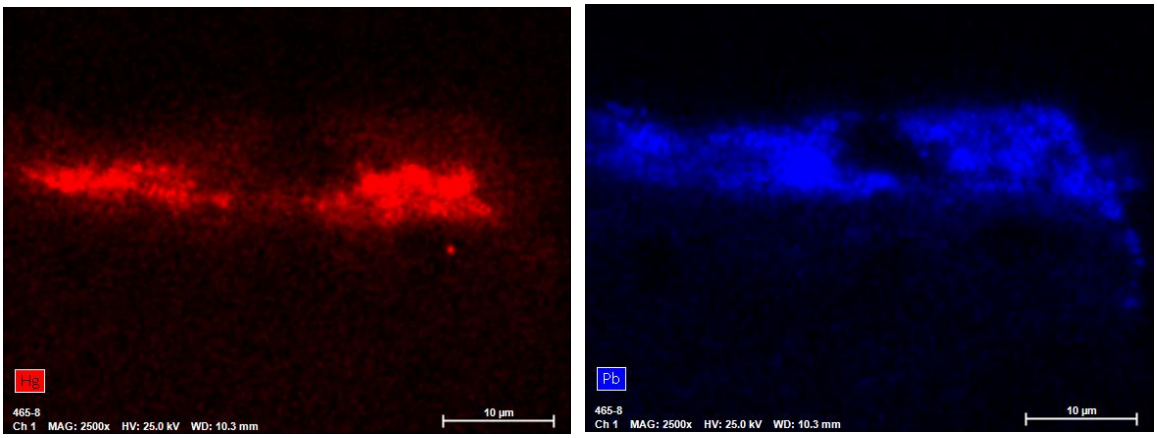


Figure A22. Hg and Pb EDS elemental maps of sample S15 cross-section.

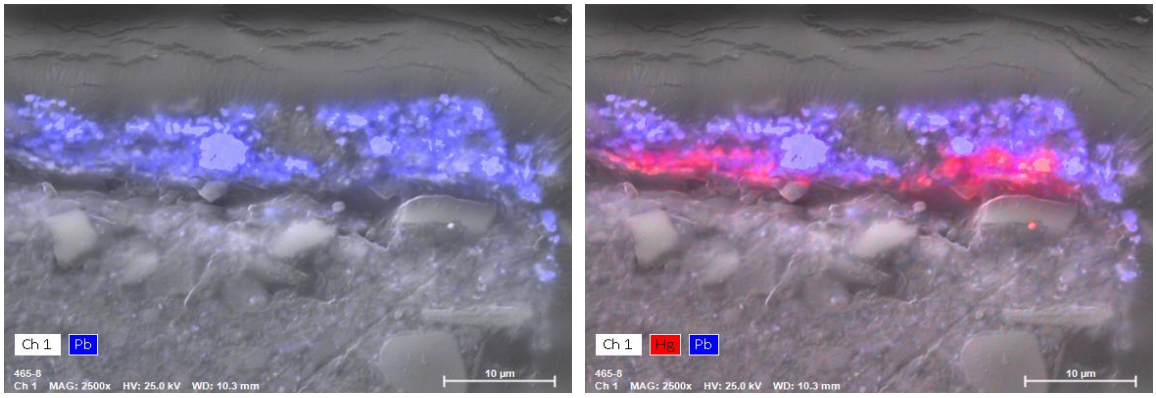


Figure A23. Pb and Hg EDS elemental maps overlaid on the SEM micrograph of sample S15 cross-section.

Appendix E

Figures A24–A30 below show the SEM-EDS spot analysis and mapping results for sample S19.

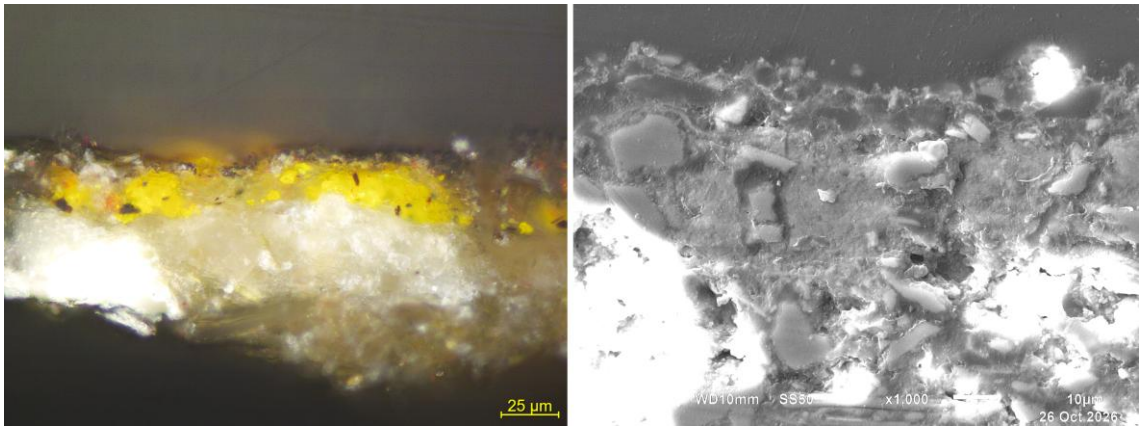


Figure A24. PLM photomicrograph (500×) and SEM micrograph (1000×) of the cross-section of sample S19.

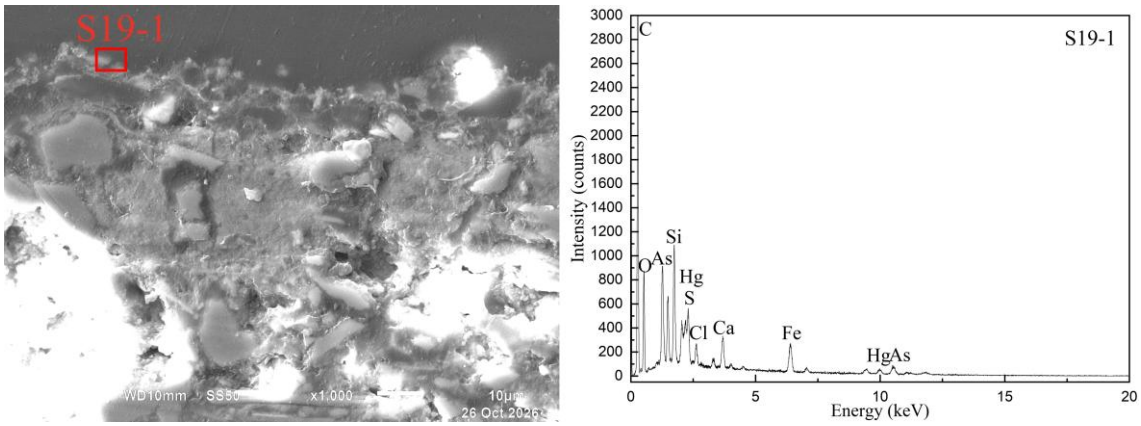


Figure A25. SEM micrograph of sample S19 cross-section and EDS area spectrum of region S19-1.

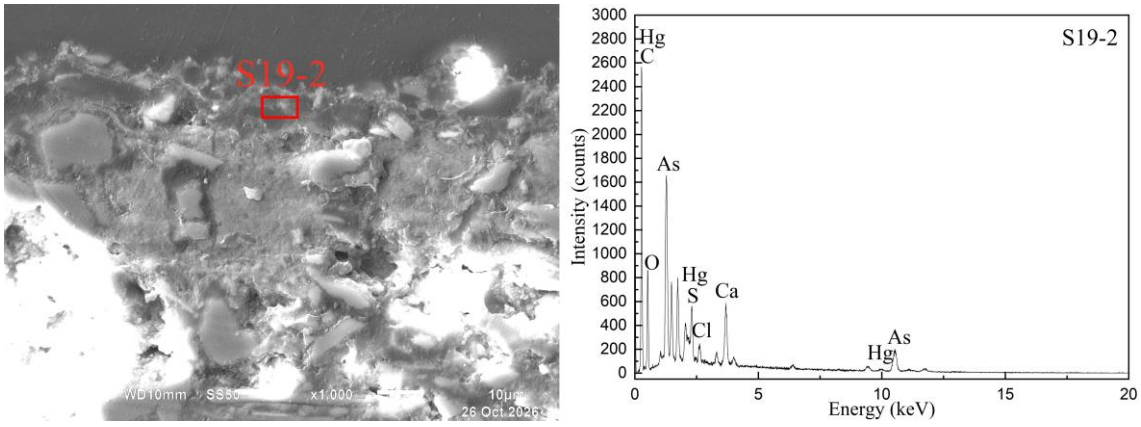


Figure A26. SEM micrograph of sample S19 cross-section and EDS area spectrum of region S19-2.

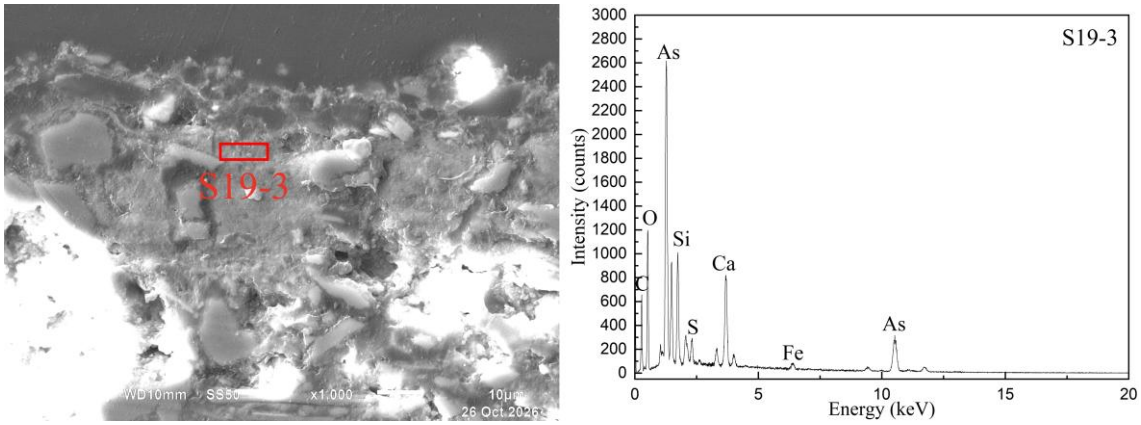


Figure A27. SEM micrograph of sample S19 cross-section and EDS area spectrum of region S19-3.

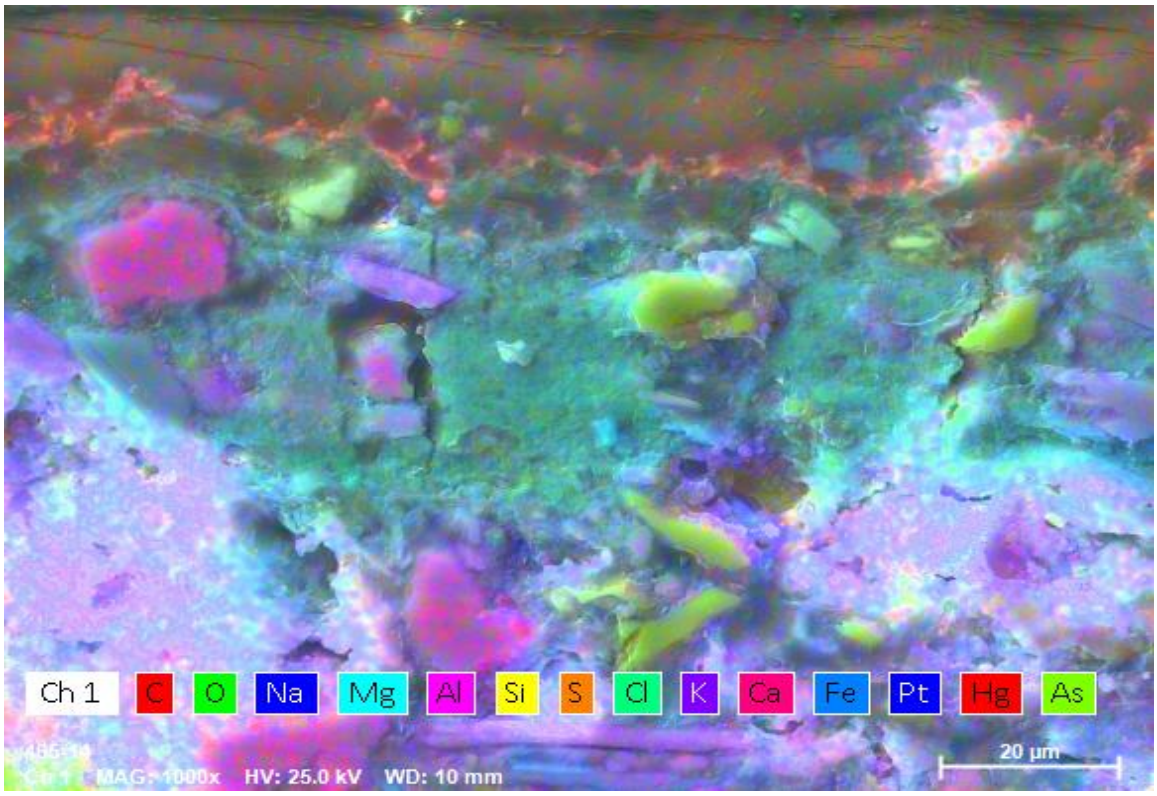


Figure A28. EDS elemental overlay map of sample S19 cross-section.

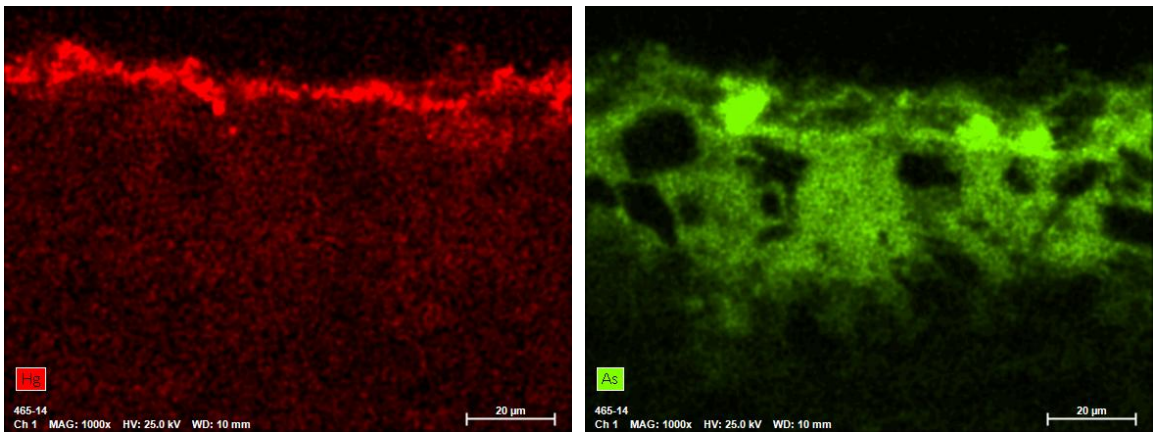


Figure A29. Hg and As EDS elemental maps of sample S19 cross-section.

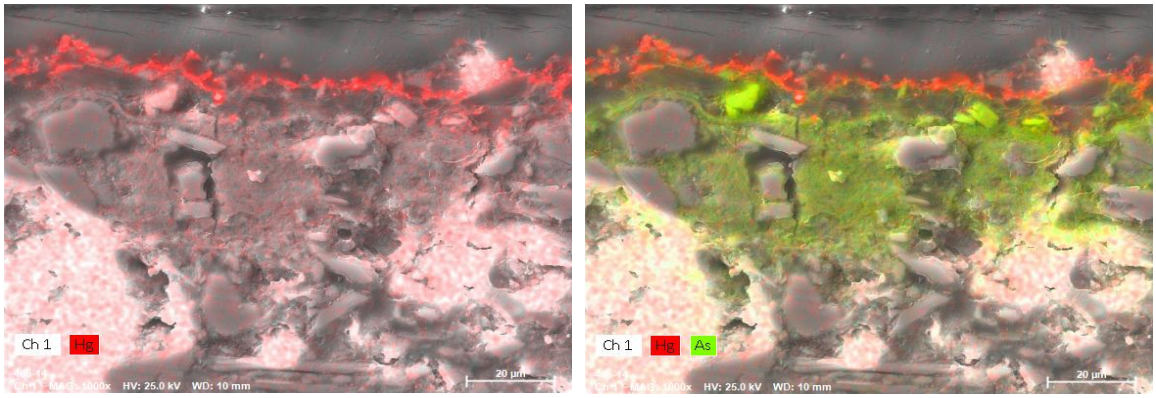


Figure A30. Hg and As EDS elemental maps overlaid on the SEM micrograph of sample S19 cross-section.

References

1. Yang, X. *Dunhuang Grotto Art: Mogao Cave 465 (Yuan Dynasty)*; Jiangsu Fine Arts Publishing House: Nanjing, China, 1996; pp. 11–29. (In Chinese)
2. Getty, A. *The Gods of Northern Buddhism: Their History and Iconography*; Dover Publications: New York, NY, USA, 1988.
3. Kossak, S.M.; Singer, J.C. *Sacred Vision: Early Paintings from Central Tibet*; The Metropolitan Museum of Art: New York, NY, USA, 1999.
4. Chandra, L. *Buddhist Iconography of Tibet*; Aditya Prakashan: Kyoto, Japan, 1986; Volume I.
5. Vira, R.; Chandra, L. *Tibetan Mandalas (Vajravali and Tantra-Samuccaya)*; International Academy of Indian Culture: New Delhi, India, 1995.
6. Rhie, M.M. An early tibetan thangka of amitayus. *Orientations* **1998**, *9*, 74–83.
7. Linrothe, R. *Ruthless Compassion: Wrathful Deities in Early Indo-Tibetan Esoteric Buddhist Art*; Serindia Publications: London, UK, 1999.
8. Yu, X.D. *A History of Tibetan Painting Styles*; Tianjin People's Fine Arts Publishing House: Tianjin, China, 2021. (In Chinese)
9. Jackson, D.P.; Jackson, J.A. *Tibetan Thangka Painting: Methods and Materials*; Shambhala Publications, Inc.: Boston, MA, USA, 1984.
10. Danba, R.D. *Tibetan Painting*; China Tibetology Press: Beijing, China, 2006. (In Chinese)
11. Lei, Y.; Wang, S.W. Material analysis of the wall paintings in Xialu Temple, Tibet Autonomous Region, China. *Stud. Conserv.* **2014**, *59*, 314–327.
12. Wang, L.L.; Li, Z.M.; Zhang, X.T.; Mei, J.J.; Ma, Q.L. A Study on the Painting Techniques of the Murals in the Prayer Corridor of Jokhang Temple, Lhasa, Tibet. *Sci. Conserv. Archaeol.* **2014**, *26*, 84–92. (In Chinese with English abstract)
13. Wu, N.; Lü, X.F.; Cuoji Meiduo. In Situ and Non-destructive Analysis of Pigments Used in an Illustrated Tibetan Manuscript Dating to the 15th Century. *China Cult. Herit.* **2021**, *4*, 87–93. (In Chinese with English abstract)
14. Pelliot, P. *Les Grottes de Touen-Houang*; Librairie Paul Geuthner: Paris, France, 1926; Volume VI.
15. Su, B. Notes on Esoteric Buddhist Remains in the Mogao Caves at Dunhuang (Part II). *Wenwu* **1989**, *10*, 68–86. (In Chinese with English abstract)
16. Jin, W.N. Artistic Remains of the Tubo Period in Tibet and Dunhuang. In *Collected Essays on Chinese Art History*; People's Fine Arts Publishing House, Beijing, China, 1981; pp. 187–189. (In Chinese with English abstract)
17. Xie, J.S. A Study on the Dating of the Murals in Mogao Cave 465 to the Western Xia Dynasty. *China Tibetol.* **2003**, *2*, 69–79. (In Chinese with English abstract)
18. Ao, T. A Synthesis Study of the Date of Cave 465 of Mogao Grottoes at Dunhuang. *Dunhuang Res.* **2003**, *5*, 3–8. (In Chinese with English abstract)
19. Xie, J.S. Identification of the Heruka and Consort Images in the Murals of Mogao Cave 465 at Dunhuang. *Dunhuang Res.* **2001**, *3*, 1–11. (In Chinese with English abstract)
20. Zhang, B.Y. A Preliminary Study of the Tibetan Buddhist Murals in Mogao Cave 465. *Tibet. Stud.* **1993**, *1*, 83–90. (In Chinese with English abstract)
21. Jin, W.N. The Discovery of the Dushashen Hall and Tibetan Inscriptions. In *Collected Essays on Chinese Art History*; People's Fine Arts Publishing House: Beijing, China, 1981; pp. 189–191. (In Chinese with English abstract)
22. Chen, H.L.; Chen, G.Q.; Xue, P.; Hou, W.F. Spatial and Temporal Distribution Characteristics of Temperature and Relative Humidity in Mogao Cave 465 at Dunhuang. *J. Arid. Land Resour. Environ.* **2018**, *32*, 155–160. (In Chinese with English abstract)

23. Kogou, S.; Shahtahmassebi, G.; Lucian, A.; Liang, H.; Shui, B.W.; Zhang, W.Y.; Su, B.M.; van Schaik, S. From remote sensing and machine learning to the history of the Silk Road: Large scale material identification on wall paintings. *Sci. Rep.* **2020**, *10*, 19312.
24. Li, D.D.; Shui, B.W.; Feng, Y.Q.; Shan, Z.W.; Yu, Z.R. Study on pigments and technological characteristics of multi-layer murals in Cave 465, Mogao Grottoes. *Res. Conserv. Cave Temples Earthen Sites* **2022**, *1*, 68–80. (In Chinese with English abstract)
25. Li, L. *Measurements and Rituals of Buddhist Images*; Shanghai Bookstore Publishing House: Shanghai, China, 2019; pp. 70–75. (In Chinese)
26. Zhao, J.L.; Yu, Z.R.; Zhang, J.K.; Song, R.Y.; Shan, Z.W.; Zhang, X.L.; Yin, Y.P.; Tan, X.; Cui, Q.; Su, B.M. Degradation mechanisms of surface coatings on polychrome clay sculptures from Zhen'guo Temple, Pingyao, Shanxi Province, China. *npj Heritage Sci.* **2026**, *in press*. https://doi.org/10.1038/s40494-026-02869-x.
27. Getty Conservation Institute. Recent Advances in Characterizing Asian Lacquer. Available online: https://www.getty.edu/projects/recent-advances-characterizing-asian-lacquer/ (accessed on 20 October 2025)
28. Zong, R.B. A Preliminary Discussion on the Color Functions of Tibetan Buddhist Painting. *Tibet. Art Stud.* **2001**, *2*, 67–70. (In Chinese with English abstract)
29. Yang, H.L. *The Art of Tibetan Painting*; Xizang People's Publishing House: Lhasa, China, 2017; pp. 172–212. (In Chinese)
30. Bhattacharyya, B. *The Indian Buddhist Iconography Mainly Based on the Sādhanamālā and Cognate Tantric Texts of Rituals*, 2nd ed; Firma K.L. Mukhopadhyay: Calcutta, India, 1958.
31. Snellgrove, D.L. *The Hevajra Tantra: A Critical Study*; Oxford University Press: London, UK, 1959; Volume 1.
32. Abhayākaragupta. Niṣpannayogāvalī (Tibetan version). In *The Tibetan Tripiṭaka: Peking Edition*; Suzuki, D.T., Ed.; Tibetan Tripitaka Research Institute: Tokyo/Kyoto, Japan, 1955–1961; Volume 80, p. 3962; rgyud 'grel, thu, fols. 115b4–185a8.
33. Gray, D.B.; Yarnall, T.F. (Translator) *The Cakrasamvara Tantra (The Discourse of Heruka): A Study and Annotated Translation*; Columbia University Press: New York, NY, USA, 2007.
34. *Bstan pa'i nyi ma phyogs las rnam rgyal. Yi dam rgya mtsho'i sgrub thabs rin chen 'byung gnas kyi lhan thabs rin 'byung don gsal [Sādhanamālā of the Panchen Lama]*; International Academy of Indian Culture: New Delhi, India, 1974; Volume 2, fol. 268b.
35. Su, B.M.; Hu, Z.D.; Li, Z.X. Study on the Stability of Mixed Red Pigments in Dunhuang Murals. *Dunhuang Res.* **1996**, *3*, 149–162.
36. Chiavari, G. Pyrolysis-gas chromatography/mass spectrometry of amino acids. *J. Anal. Appl. Pyrolysis* **1992**, *24*, 123–137.
37. Wang, N.; Gu, A.; Min, J. Identification of protein binding media used in Chinese cultural relics by Py-GC/MS. *Chin. J. Anal. Chem.* **2020**, *48*, 90–96. (In Chinese)

Disclaimer/Publisher's Note: The statements, opinions and data contained in all publications are solely those of the individual author(s) and contributor(s) and not of MDPI and/or the editor(s). MDPI and/or the editor(s) disclaim responsibility for any injury to people or property resulting from any ideas, methods, instructions or products referred to in the content.